USGS Award No. G18AP00064
Award Period: 07/01/2018 – 12/31/2019

SIMULTANEOUS RAYLEIGH AND LOVE WAVE ACQUISITION FOR JOINT INVERSION OF MASW DATA

Principal Investigators:

Joseph Thomas Coe, Jr., Ph.D.
Department of Civil & Environmental Engineering
Temple University, 1947 North 12th Street, ENGR Building Room 518
Philadelphia, PA 19122-6018
Office: (215)204-6100, Fax: (215)204-4696, joseph.coe@temple.edu

Graduate Student Researchers:

Trumer Wagner
Department of Civil & Environmental Engineering
Temple University, 1947 North 12th Street
Philadelphia, PA 19122-6018
tuf53109@temple.edu

Siavash Mahvelati
Department of Civil & Environmental Engineering
Temple University, 1947 North 12th Street
Philadelphia, PA 19122-6018
smahvelati@temple.edu

Final Technical Report

September 23, 2021

Project Website: https://sites.google.com/a/temple.edu/joseph-coe/research/usgs-g18ap00064

ACKNOWLEDGEMENT OF SUPPORT AND DISCLAIMER

This material is based upon work supported by the U.S. Geological Survey under Grant No. G18AP00064. The views and conclusions contained in this document are those of the authors and should not be interpreted as representing the opinions or policies of the U.S. Geological Survey. Mention of trade names or commercial products does not constitute their endorsement by the U.S. Geological Survey.

The authors would like to thank former Temple University Ph.D. student Alireza Kordjazi and former Temple University M.S.C.E. students Philip Asabere and Michael Senior for their assistance during field testing. The authors would also like to thank Dr. Laura Toran for her input regarding the location of the monitoring wells at the Temple University Ambler site. GISCO provided the ESS Mini AWD source used in this study and their support for our research team is greatly appreciated.

TABLE OF CONTENTS

LIST OF FIGURES

LIST OF TABLES

Preface: The contents of this report have been adapted from: Wagner, T. (2020). *Simultaneous Rayleigh and Love Wave Generation for MASW Data.* M.S. Thesis, Temple University. All project files can be located at: https://sites.google.com/a/temple.edu/joseph-coe/research/usgs-g18ap00064

ABSTRACT

The Multichannel Analysis of Surface Waves (MASW) method continues to increase in popularity as a tool to characterize subsurface stiffness for site characterization. In typical MASW testing, a linear array of geophones is used to record the surface waves generated from either vertical impacts (Rayleigh waves) or horizontal impacts (Love waves). The phase velocity of these surface waves is frequency-dependent in a vertically heterogeneous domain. This velocity-frequency dependency (i.e., the dispersion curve) can be examined by applying wavefield transforms to the recorded raw signals. An inversion algorithm is then implemented that attempts to locate the most probable shear wave velocity (Vs) profile by matching the measured dispersion curve with theoretical dispersion curves generated from forward modeling. This process is inherently nonlinear and ill-posed, without a unique solution. As a result, considerable research has been devoted to inversion algorithms for MASW. A number of studies have explored joint inversion of Rayleigh (MAS_RW) and Love (MAS_LW) waves as a means to improve the accuracy of V_S profiles. However, Rayleigh and Love waves are routinely generated with a different source, which increases the length of time for data acquisition to switch sources and reacquire data. No studies have systematically examined the capabilities to develop simultaneous Rayleigh and Love waves from single sledgehammer impacts on the same angled or vertical base plate source. Such an approach could encourage the use of joint inversion schemes for MASW due to increased data acquisition efficiency. This research project addresses this limitation by exploring optimal techniques for generating simultaneous Rayleigh and Love waves (i.e., $MAS_{RL}W$) for use in joint inversion.

In this study, MASW field testing was performed to examine the effectiveness of an angled impact for the simultaneous generation of Rayleigh and Love waves. Testing was performed at a baseball field at the Temple Ambler campus site (TAB) approximately 24 km north of Center City Philadelphia. A set of 24 geophone receivers was used to collect surface wave data from impacts were performed at angles of 0°, 15°, 30°, 45°, and 90°. Both independent and joint inversions were performed to produce V_S profiles from the data. These V_S profiles were subsequently compared to ground truth information obtained from previous seismic refraction and downhole testing. Additionally, the waveforms were examined with respect to spectral content and signal-to-noise ratio and the dispersion images/curves were also compared. The results of this study demonstrated that Love waves were significantly less affected by changes in impact angles when compared to Rayleigh waves. Consequently, the optimal angle for simultaneous generation of Rayleigh and Love waves may be biased more towards vertical. In this case, an impact angled at 15° from vertical proved to be the best configuration for simultaneous generation of Rayleigh and Love waves.

1. INTRODUCTION

The behavior of a soil is directly related to its geotechnical properties such as stiffness [i.e., small strain shear modulus (G_0)]. The G_0 of a soil is a critical input parameter in several seismic design applications, including estimation of ground motions and liquefaction potential. Typically, seismic geophysical methods can be used to measure the shear wave velocity, V_S, of the soil as a proxy for G_0 since it is directly related to G_0 by mass density ($G_0 = \rho V^2$).

Geophysical methods that estimate V_S without drilling or invasive procedures (i.e., non-destructive methods) have been increasingly used instead of traditional downhole and crosshole methods that are more time intensive and costly. Surface wave analysis is a type of non-destructive geophysical test that has been increasing in popularity since its development in the 1990s (Park et al., 1999; Xia et al., 1999). A surface wave is a wave that results from the interaction between body waves (P-waves/primary waves and S-waves/secondary waves) and propagates along the interface between two different media (Figure 1.1). The two main types of surface waves are Rayleigh and Love waves, which develop different particle motions in the underlying subsurface. The velocity of both Rayleigh and Love waves are dependent on V_S and can therefore be used to determine its variation with depth at a site.

Rayleigh waves, the most fundamental of the surface waves, propagate in the vertical direction and have a motion similar to that of a rolling ocean wave (Figure 1.1). The propagation of Rayleigh waves depends on the wave frequency, V_S, primary wave (P-wave) velocity (V_P), layer thickness, and soil density (ρ) (Xia et al., 1999). For Rayleigh waves, the amplitude of the associated motion decays exponentially with depth. This motion becomes negligible within about one wavelength (λ) from the surface, where λ is related to the frequency (f) of the wave and its phase velocity (V) by $\lambda = V / f$. The decay of particle motion amplitude with depth for a Rayleigh wave cannot be predicted a-priori without knowledge of the subsurface structure (Foti et al., 2017).

The particle motion of a Love wave is horizontal and transverse to the direction of wave propagation (Figure 1.1). Love wave propagation depends on the same parameters as Rayleigh waves, except for V_P due to the purely horizontal particle motion. Love waves exist only in media where there is a soft layer overlaying a stiffer layer, whereas Rayleigh waves always exist where there is a free surface.

Surface wave testing has evolved from its origins with the early pioneering work of the 1950s (Van de Pol 1951; Jones 1955) and single receiver approaches (Abbiss, 1981; Tokimatsu et al., 1991; and Matthews et al., 1996) through multi-receiver approaches (e.g., Heisey et al., 1982). The most recent breakthrough in surface wave testing came with the introduction of the Multichannel Analysis of Surface Waves (MASW) method by Park et al. (1999) and Xia et al. (1999). In this method, surface waves are generated at a site and recorded by a large number (i.e., 24 or more) of receivers (Figure 1.2). The MASW method consequently allows for more efficient data acquisition and for faster and more easily automated data processing. Noise sources, such as inclusion of body waves and reflected/scattered waves can be more easily filtered out, which can lead to a more accurate V_S profile than other surface wave methods (Ólafsdóttir, 2014). Furthermore, observation

of more complex wave propagation characteristics and generation of two (or three) dimensional velocity profiles becomes possible and economically feasible.

All surface wave methods attempt to decipher the characteristics of the subsurface by examining the dispersive nature of the recorded surface waveforms. Dispersion refers to the phenomenon whereby different *f* components of the waveforms (i.e., different λ) "sample" different depths of the subsurface and therefore propagate at different *V*. Once the dispersion behavior of the waveforms has been established at the site, an inversion problem is solved to generate a subsurface velocity model. The inversion proceeds by attempting to match the acquired dispersion information with theoretical dispersion information from forward modeling with various trial subsurface velocity profiles.

1.1. Problem Statement

Traditionally, MASW has been performed using the generation of Rayleigh waves (i.e., MAS_RW or MARW). The application of Love waves to MASW (MAS_LW or MALW) has only recently gained traction (Yong et al., 2013) despite knowledge of their existence since the start of the 20th century (Love, 1911). There are a number of advantages presented by use of Love waves in surface wave surveys, including independence from V_P, higher signal-to-noise ratio (*SNR*), and a more stable inversion process (Xia et al., 2012). Love wave surveys can be performed to supplement Rayleigh wave surveys. In this scenario, two separate V_S profiles would be generated that could be used to increase the accuracy of the predicted subsurface characteristics and bracket the final solution. Alternatively, the two sets of dispersion information from recordings of Rayleigh and Love waveforms can be jointly inverted. The purpose of joint inversion is to develop one objective function to optimize during the inversion process. This singular objective function is jointly developed from the individual objective functions representing the Rayleigh and Love wave data sets. In this manner, joint inversion can reduce the number of acceptable subsurface velocity models and can produce mutually consistent estimates because the results must explain all data simultaneously (Vozoff and Jupp, 1975; Julia et al., 2000).

Whether Love waves and Rayleigh waves are independently or jointly inverted, the supplemental use of Love waves for MASW is desirable to increase the accuracy of predicted subsurface stiffness. However, Rayleigh and Love waves propagate most strongly in directions perpendicular to one another – Rayleigh waves in the vertical direction and Love waves in the horizontal direction. Consequently, Rayleigh and Love waves are typically generated by separate vertical and horizontal impacts on the ground surface, respectively (Figure 1.3). A metallic base plate is typically used to couple the impact energy and improve its transfer into the underlying ground surface. The configuration of this base plate is different between Rayleigh and Love wave generation due to the orientation/polarization of the impact (Figure 1.3). Therefore, Rayleigh and Love waves are almost always generated and recorded separately if both sets of waves are used. This results in conducting twice as many impacts to obtain the data necessary for the analysis of both Rayleigh and Love waves. So, while MASW using both Rayleigh and Love waves (i.e.,

$MAS_{RL}W$ or MARLW) may increase the accuracy of the velocity profile compared to single-component MASW, the time and effort of data collection is significantly increased and both sets of waves are rarely used.

If Rayleigh and Love waves are generated and recorded simultaneously from the same impact, the efficiency of the data acquisition process is drastically improved. In return, $MAS_{RL}W$ becomes a more appealing process due to the benefit of increased accuracy with minimal changes to analysis time and/or effort. However, very little research has been performed to systematically analyze the most effective impact angle with which to simultaneous generate Rayleigh and Love waves as highlighted in the literature review of Chapter 2. Consequently, no guidance exists about how to design the most appropriate $MAS_{RL}W$ survey, particularly with respect to the manner with which the seismic source is used to simultaneously generate the waves.

1.2. Scope of Research

Given the aforementioned gaps in the literature regarding simultaneous generation of Rayleigh and Love waves, this research project addresses the following issues:

1. What is the optimal angle of impact for simultaneous generation of Rayleigh and Love wave generation.
2. How effective are vertical impacts for generating simultaneous Rayleigh and Love waves.

This research efforts aims to advance the field of geophysical subsurface investigation, specifically MASW testing. By improving the accuracy and data collection times of MASW, the procedure will continue to increase in popularity and offer an appealing alternative to traditional geotechnical subsurface investigation methods.

As noted previously, Rayleigh waves are typically generated using a vertical impact (i.e., 0° angle from a line drawn vertically from the ground surface) of a sledgehammer (Figure 1.3). Love waves are typically generated using a completely horizontal impact (i.e., 90° angle from a line drawn vertically from the ground surface) (Figure 1.3). Any deviations from these "ideal" Rayleigh and Love impact sources and angle should result in negative effects on several characteristics of the recorded signals, including *SNR*, spectral content, and perhaps the accuracy of the resulting V_S profile. Selection of an optimal angle of impact should therefore represent an intermediate angle between 0° to 90° that least negatively affects both types of waveforms.

In theory, an impact angle of 45° should represent the optimal angle for the simultaneous generation of Rayleigh and Love waves since approximately half of the impact energy is converted into Rayleigh waves and the other half Love waves. Impact angles closer to vertical would likely generate a higher proportion of Rayleigh wave energy at the expense of Love wave energy. Impact angles closer to horizontal would likely improve Love wave performance at the expense of Rayleigh waves. However, it is not clear whether there is some aspect of either Rayleigh or Love wave generation that reduces their sensitivity to the impact angle. In such a scenario, the optimal

impact angle may be controlled by one waveform over another. For example, if Love waves are less sensitive to impact angles and only a minimum threshold is needed to generate adequate Love wave energy, the optimal impact angle would be controlled by a bias towards generating more Rayleigh wave energy.

In this study, the optimal impact angle was examined on the basis of *SNR*, relative energy, frequency content, and dispersion information. Additionally, the final V_S profiles created by angled impacts were compared with V_S profiles produced from ground truth information. The goal of this research effort is to identify an impact angle that generates V_S profiles that compare favorably to those created from traditional MAS_RW and MAS_LW techniques and to those representing ground truth. Based on these efforts, it may be possible to provide prescriptive guidance for optimal field efforts with simultaneous generation in the future.

In addition to attempting to identify the optimal impact angle for simultaneous generation of Rayleigh and Love waves, this study also evaluates the effectiveness of vertical impacts for this same purpose. The research question being tackled in this phase of the study is whether a purely vertical impact can generate sufficient Love wave energy for analysis in either an independent inversion process or joint inversion algorithm. Though it may seem odd to consider that a purely vertical impact may generate horizontally-polarized wave energy, gravitational forces may indeed cause a very small proportion of a vertical impact to convert into some form of horizontal wave propagation. Vertical impacts for Love waves will likely never produce the same quality data as horizontal impacts, but usable data may still be obtained from such strikes. As noted in the Chapter 2 literature review, there is some empirical evidence from other studies that such a small component of horizontally-polarized waveform energy is measurable using modern receivers and data acquisition systems. Consequently, it may be possible to forgo the use of specialized horizontal base plates in favor of a standard metallic base plate as used with Rayleigh wave generation. This would simplify data acquisition and further encourage the use of $MAS_{RL}W$ in lieu of MAS_RW and/or MAS_LW. This task was also evaluated based on *SNR*, relative energy, frequency content, dispersion information, and accuracy of the inverted V_S profile.

1.3. Organization of Topics

The scope of this research is to examine the role of impact angles on the simultaneous generation of Rayleigh and Love waves for MASW testing. The body of this report is organized into the following chapters:

- Chapter 2: Background and Literature Review
  This chapter summarizes the relevant general background on surface wave testing and the specifics related to the MASW methodology itself. A discussion is provided regarding the role of data acquisition, post-processing, and subsequent inversion on MASW results. A comprehensive literature review is also presented that discusses relevant studies on simultaneous generation of Rayleigh and Love waves.

- Chapter 3: Data Collection and Processing
  Chapter 3 describes the efforts to acquire the surface wave data at the selected field site. The field site itself is initially described as well as previous testing performed to characterize ground truth. The specifics of data acquisition are presented as well as how the data was post-processed and analyzed for *SNR*, spectral content, dispersion information, and inverted V_S profile.

- Chapter 4: Analysis of Results and Discussion
  This chapter presents the findings from the field testing performed in this study. The effects of base plate are examined with respect to *SNR*, spectral content, dispersion information, and resulting V_S estimates.

- Chapter 5: Conclusions and Recommendations
  Chapter 5 summarizes the important findings from the field testing performed in this study. Recommendations are provided regarding the role of impact angle on simultaneous generation of Rayleigh and Love surface waves for MASW testing.

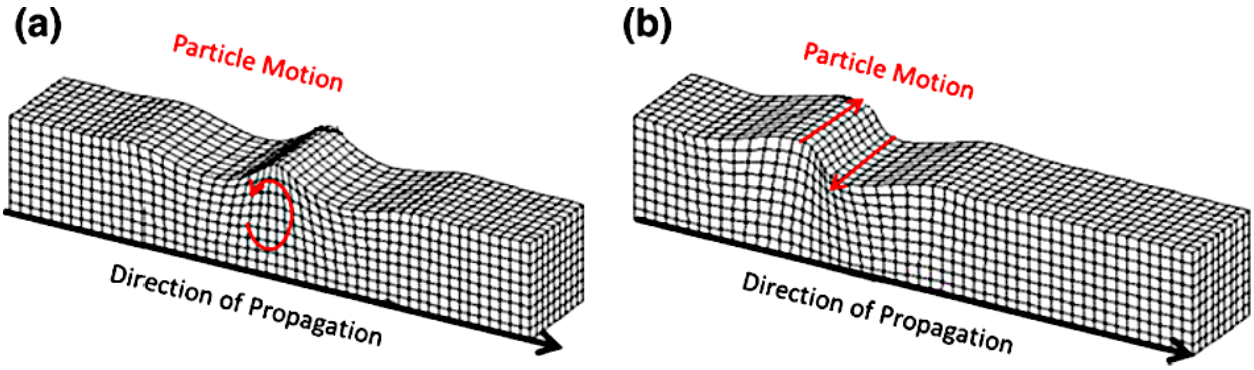

Figure 1.1. Direction of wave propagation for (a) Rayleigh and (b) Love waves. (Foti et al., 2017).

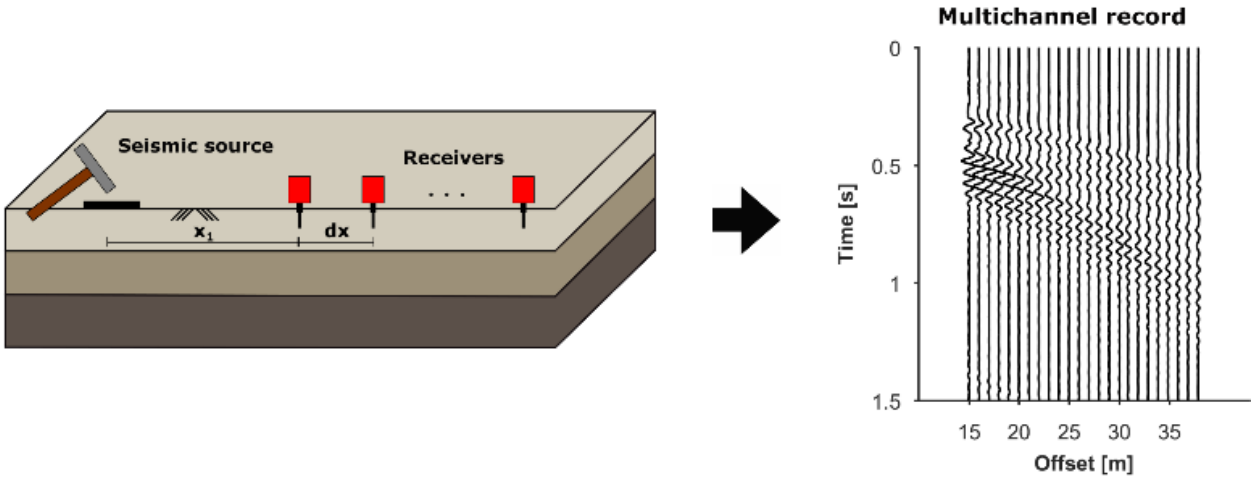

Figure 1.2. MASW data acquisition and resulting multichannel record with surface waves (adapted from Olafsdottir et al., 2018).

(a) **(b)**

Figure 1.3. Generation of (a) Rayleigh waves, and (b) Love waves for MASW.

2. BACKGROUND AND LITERATURE REVIEW

Surface wave analysis aims to generate a shear wave velocity (V_S) profile by solving an inverse problem of model parameter identification based on an experimental dispersion curve. Typical analysis procedures consist of three sequential steps: (1) acquisition of seismic data; (2) data post-processing (dispersion curve estimation); and (3) inversion (model parameter optimization) (Foti et al., 2017) (Figure 2.1). The following sections describe these steps in more detail. More specific details of the MASW methodology adopted for this study is subsequently presented.

2.1. Surface Wave Dispersion

Surface wave propagation is controlled by dispersion; that is, waves of different wavelengths (λ) "sample" different depth ranges and the corresponding phase velocity (V) depends on the material properties of the subsurface within that wave's propagation range (Foti et al., 2017). Love waves are inherently dispersive while Rayleigh waves are only dispersive in a heterogenous media. This means that the V of wave propagation is dependent on the frequency (f) of the wave. Surface wave methods measure this f dependency of surface wave V (i.e. dispersion). After data collection and processing, the first step toward creating a V_S profile is the generation of a dispersion image. The end product is a V_S profile that is estimated using an inversion process to match field dispersion measurements to theoretical curves generated using forward modeling.

The parameters f, V, and λ are related by the equation $f = V / \lambda$. Therefore, for the same V, lower f equates to a higher (longer) λ, and vice-versa. Long λ surface waves penetrate more deeply into the subsurface than short λ surface waves (Figure 2.2). Since the V of wave propagation in the Earth tends to increase with increasing depth, the longer λ (low f) waves can travel faster than the shorter λ (high f) waves. These relationships are used to generate the dispersion curve for a subsurface.

2.1.1 Development of Dispersion Curves

One of the most important aspects of surface wave testing is the development of a dispersion curve based on the input seismic wave. The dispersion curve characterizes the *V-f* behavior of the surface waves at a site. Several signal analysis tools can be used for the extraction of dispersion curves from experimental data. Methods that can be implemented to provide an automated extraction of the dispersion curve are helpful, but a careful assessment of obtained information is necessary (Foti et al., 2017). Most of these techniques assume a one-dimensional medium below the array (horizontally stratified, V only varies with depth), and plane wave propagation (the receiver array is far enough from the seismic source so that the surface wave is fully developed and the wave front can be approximated by a plane) (Foti et al., 2017).

Visual inspection of the dispersion curve can provide an indication of the expected trends in the V_S profile. A dispersion curve with a smooth and continuous decrease of V for increasing f is typically associated with simple stratigraphic conditions with V_S consistently increasing with depth (i.e. a normally dispersive subsurface). The presence of a dip in the experimental dispersion curve can indicate the presence of an inverse layering at some depth (i.e. a soft layer below a stiffer one) (Foti et al., 2017).

Several techniques exist for the analysis of the seismic data and creation of a dispersion image. The multichannel record, which is in the time (t)-space (x) domain, is converted into either the frequency (f)-wavenumber (k) or the frequency (f)-phase velocity (C_f) domain (e.g., McMechan and Yedlin 1981; Park et al. 1998). The resulting dispersion image (Figure 2.1) represents the patterns of energy accumulation resulting from the wavefield transformation.

2.1.1.1 Phase-Shift Method

The quality of the dispersion image generated by the phase-shift method (Park et al., 1998) is superior to those obtained by the other aforementioned methods. Therefore, the phase-shift method was used throughout this research effort to develop dispersion images. In the phase-shift method, the dispersion properties of all types of waves contained in the recorded data are visualized in the f-C_f-transformed energy (summed wave amplitude) domain (Olafsdottir, 2014). The phase-shift method can be divided into three steps:

1. Fourier transformation and amplitude normalization
2. Dispersion imaging
3. Extraction of dispersion curves

As described by Park et al. (1998), in the phase-shift method, the raw field data in the offset-time domain are first transformed via Fast Fourier Transform (FFT) into individual f components (offset-frequency domain), and then amplitude normalization is applied to each component. The new domain is a combined function of amplitude and phase spectra. The amplitude part of the offset-frequency domain contains properties of attenuation, spherical divergence, and related information, whereas the phase spectra explain the wave dispersion (Park et al. 1998).

Next, for each offset at a given C_f and f in a certain range, the phase shift required to compensate for the time delay corresponding to that specific offset is calculated and applied. Next, at particular f intervals (i.e., 1 Hz intervals), the transformed traces (offsets) are aggregated using an integral function (Park et al. 1998). At each f, there is a C_f providing a maximum value for the accumulated energy presented by the integral. This represents the C_f (or V in previous terminology) at that particular frequency. The display of all summed energy in the f-C_f space highlights a pattern of energy accumulation that represents the dispersion curve.

2.1.1.2 Modes of Surface Wave Propagation

In a horizontally layered medium, surface wave propagation is a multimodal phenomenon. That is, at each *f*, different modes of vibration exist that can make the dispersion curve multi-modal. The mode with the lowest C_f (at each *f*) is termed the fundamental mode. Higher modes, also known as first mode, second mode, etc., have higher C_f that are only present above a cut-off *f* that depends on the mode (Olafsdottir, 2014). It is necessary to pick the relative maxima of the spectrum and associate them to the fundamental or defined higher mode (Foti et al., 2017).

The existence of higher modes of surface waves is due to constructive interference phenomena occurring among waves undergoing multiple reflections at the layer interfaces (Foti et al., 2017). Different overtones carry different energy, making them not always detectable (i.e. only a few modes may be excited). Energy distribution is also *f*-dependent. A mode can be strongly dominating within a certain *f* band, while negligible in other bands. Energy distribution is controlled by many factors: primarily the site-specific velocity and attenuation (i.e. wave amplitude loss), in combination with the source type, location, and coupling with the ground (Foti et al. 2017). Commonly, the propagation is determined by the fundamental mode. In some cases, however, particularly where very strong velocity contrasts exist between layers at shallow depths, or where a low-velocity layer exists between two high-velocity layers, higher modes may be excited and need to be used in the inversion analysis (Foti et al., 2017). Given the complexities involved with identifying the appropriate higher mode, a fundamental mode dispersion curve is typically extracted from the overtone image and subsequently used in the inversion process to estimate V_S.

2.2. Inversion

Once an experimental dispersion curve has been selected from the acquired data, an inversion algorithm is used to determine the V_S profile of the site. The goal of the inversion process is to identify the subsurface model whose forward response best fits the experimental data. During the inversion process, a model parameter identification problem is solved by using the experimental dispersion curve(s) as the target. The subsurface is typically modeled as a stack of horizontally layered elastic and isotropic media (Foti et al., 2017). The resulting profile gives the V_S structure that is most representative of the subsurface material below the receiver spread. Each of the layers is characterized by four parameters: thickness (t), mass density (ρ), Poisson's ratio (ν), and wave velocities. By using a-priori assumptions about ρ and ν, the unknown model parameters are often restricted to t and V_S.

Inversion procedures can be divided into two broad categories: local and global search methods. The goal of these processes is to find a subsurface model that best fits the experimental (measured) data. During the local search method (LSM), a theoretical model is generated based on estimates of subsurface parameters (e.g. V_S, layering, and ρ) and then compared with the experimental model (Figure 2.3). Typically, the Root Mean Square Error (RMSE) is used to calculate the amount of

misfit between the theoretical and experimental model. Theoretical models are generated until there is an acceptably low difference between the experimental and theoretical models. LSM are efficient in regard to both time and computational power, but because the solution is based on a pre-defined starting model, there is a risk of the model becoming stuck at a local minimum during the inversion process (Socco et al., 2010). The choice of the initial model is therefore crucial in LSM because the result of the inversion may be strongly dependent on the adopted initial model (Foti et al., 2017).

In global search methods (GSM), a probability density distribution is defined for each model parameter, creating a range for potential models (Foti et al., 2017). A conventional approach to global search is to randomly generate parametric sets within the previously specified range. In contrast with the single model produced by local search methods, GSM generate a set of acceptable profiles. GSM require significantly more time and computational power compared to local search methods but have the potential to produce more accurate V_S profiles.

2.3. Uncertainty in Surface Wave Methods

A key issue with surface waves is the uncertainty associated with the inversion process. The final model is affected by solution non-uniqueness, as several theoretical dispersion curves may provide a similar match to the experimental curve (Foti et al., 2017). The result of the inversion process is inherently ill-posed (the solution's behavior does not depend continuously on the initial conditions), non-linear (the change in the solution is not proportional to the change in the initial conditions), and mix-determined (insufficient data is available to constrain certain model parameters) (Cox and Teague, 2016).

GSM mitigate some of the issues of uncertainty associated with MASW and are recommended to be used when no a-priori information is available. These methods avoid assumptions of linearity between the observables and the unknown and offer a way of handling the non-uniqueness of the inversion problem (Socco et al., 2010). GSM are gaining popularity due to continued improvements in computational power and the development of several optimization methods. These optimization methods utilize simulated annealing (SA) or apply genetic algorithms (GAs) to reduce the number of simulations required to obtain a best fit.

A-priori information about the subsurface site conditions may also increase the accuracy of the V_S profile by restricting the model parameters to a range of reasonable values. Any available a-priori information should be factored into the initial parameterization for both local and global search methods. Useful information can be retrieved from previous studies, geological maps, borehole data, or other geophysical tests. Unfortunately, a-priori site information is often difficult to obtain, especially at depths where surface wave testing resolution and accuracy suffers. Consequently, many MASW inversion are performed in a "blind" fashion.

The inclusion of higher modes during the inversion process presents another means of obtaining a more accurate V_S profile. Typically, a fundamental mode (i.e., lowest C_f for a given f) is selected

from the peak intensity values plotted in the dispersion image. However, there has been significant debate regarding the importance of higher modes of propagation. It is now recognized that higher modes play a significant role in the inversion process and failing to consider them may cause errors in several situations (Socco et al. 2010 and Xia et al. 2000). Joint inversion of the fundamental and higher modes produces additional independent information that is useful to combat solution non-uniqueness. While several methods have been proposed to account for higher modes during inversion, the procedures are not standardized or implemented in most commercial codes (Foti et al., 2017).

2.4. Fundamentals of the MASW Methodology

During MASW, surface waves are generated by active methods, such as a sledgehammer striking a baseplate, or by passive methods, such as ambient traffic vibrations (Figure 2.1). These active and passive sources provide various levels of excitation and signal quality. Typically, a larger, heavier source generates longer λ while a smaller, lighter source produces shorter λ. A receiver such as a geophone senses the ground vibration generated by the surface wave and converts that vibration into electric current via a mass-spring system enclosed in a magnet. The *f*-amplitude relationship of a geophone is called the "response curve" and is determined primarily by the size of the hanging mass and stiffness of the spring. Vertical geophones are used for Rayleigh wave surveys while horizontal geophones are used for Love wave surveys. The raw waveforms are recorded by a field device, typically a seismograph. The data is then processed, analyzed, and used to create a V_S profile of the subsurface. These steps are further discussed in the following sections.

2.4.1 MASW Field Procedures

The first step toward generating a V_S profile with MASW is data collection. Surface waveforms may be collected by two primary methods: active and passive surveys. During an active survey, surface waves are generated by sledgehammer strikes on a baseplate. In passive surveys, ambient surface waves are collected from background seismic sources such as traffic. The depth of investigation is directly proportional to the longest measurable λ (lowest *f*) and the minimum resolvable layer thickness is related to the shortest λ (highest *f*) (Xia et al., 1999; Park et al., 2002). The maximum measured λ depends on (Foti et al., 2017):

- The frequency content of the propagating seismic signal
- The array layout aperture used for recording
- The frequency bandwidth of the sensors
- The velocity structure of the site

Data acquisition up to a depth of 30 m using a sledgehammer is typically only possible for stiff sites; soft sites generally have a maximum investigation depth of 15-20 m with a sledgehammer. Background ambient surface wave vibrations can typically investigate deeper strata because they

generally contain lower *f* content than even the largest active seismic sources. Consequently, it is recommended that both active and passive surveys be performed at sites where the target investigation depth is greater than approximately 20-25 m (Foti et al., 2017). Field acquisition parameters can have a significant impact on data quality and are, therefore, designed to adapt the above characteristics to the project objective.

2.4.2 Seismic Source

During active MASW testing, surface waves are generated by a seismic source. This source must provide an adequate signal-to-noise (*SNR*) ratio over the required frequency band, given the target investigation depth. Since wavelength is a function of both *f* and *V* (i.e., C_f), it is necessary to make initial estimates regarding the expected velocity range to define the required *f* band of the source. At a soft site, lower *f* will be necessary to achieve the same investigation depth as at a stiff site. Vertical operated shakers or vertical impact sources are typically used for surface wave testing. Shakers provide accurate control of *f* and a very high *SNR* in the optimal frequency band of operation. However, they are also very expensive and difficult to manage. Impact sources, on the other hand, are much cheaper and still enable as efficient data acquisition as shakers over a wide frequency band.

The cheapest and most common source is a sledgehammer striking a metal plate or directly on the ground surface. However, the sledgehammer is typically limited to f > 8-10 Hz, which limits investigation depth to a few tens of meters (typically no more than 30 m). Accelerated weight drop (AWD) sources can improve the low *f* response and investigation depth since they typically generate more energy than sledgehammer sources. Additionally, they offer repeatability with respect to the energy introduced by each impact. However, AWD units are large, cumbersome to deploy, and expensive. As with any active source, the *SNR* can be improved by stacking multiple shots. Additionally, the energy output of the sledgehammer is dependent on its operator. Precautions must be taken to ensure the quality of data is not altered by varying sledgehammer strikes.

A trigger switch is typically used to begin data acquisition. This trigger switch may be attached to the source (e.g. taped to the sledgehammer) or placed very close to the source so as to trigger before the surface waves reach the geophone array.

2.4.3 Receivers

Geophones are commonly used as receivers for acquisition of Rayleigh and Love wave data during MASW testing. The geophone must be capable of recording vertical motions to acquire Rayleigh waveforms and horizontal geophones are used to record Love waves. Single component geophones (i.e., only vertical or horizontal polarization) are commonly used, though multi-component geophones are available and decrease data acquisition times for investigations where both

Rayleigh and Love waves are used. MASW is typically performed using 24 or 48 geophones, though this is limited by site logistics and costs more than anything. The geophones may be planted into soft to medium-stiff ground via spikes or placed on flat bases (typically metallic).

The natural *f* of the geophones must be adequate to sample the expected frequency band of surface waves without distortions due to sensor response. Generally, for shallow targets (e.g. 30 m) 4.5 Hz geophones are typically used for both MAS_RW and MAS_LW. For active surveys, the geophones are equally spaced in a straight line from the source. During passive surveys, it is common practice to arrange the geophones in a 2D array on the ground surface in order to capture ambient vibration from any direction. However, the straight-line configuration is also used for passive surveys with longer receiver spacings to adequately capture the longer λ for the ambient vibrations. Lower *f* geophones (e.g., 1 Hz) may be used to acquire the longer λ (i.e., lower *f*) signals.

The array length for active surveys should be adequate for a reliable sampling of long λ, which are associated with the propagation of low-frequency components. A rule of thumb is to have the array length at least equal to the maximum desired λ, which corresponds to approximately twice the desired investigation depth (Foti et al., 2017). The spacing between adjacent receivers should be adequate to reliably sample short λ, which are associated with the high-frequency waves necessary to constrain the near-surface solution. Suggested values for receiver spacing range from 0.5 m to 4 m (Foti et al., 2017).

The source position should be selected as a compromise between the need to avoid near-field effects, which prevent surface waves from fully developing, and the opportunity to preserve high-frequency components that rapidly degrade with distance as a result of far-field effects. It may be useful to repeat MASW acquisition with multiple source offsets and source types to ensure high-quality data. Stacking of multiple shots is also good practice, as it increases the *SNR* and therefore improves the phase velocity estimation.

2.4.4 Acquisition Device

A variety of devices may be used to digitize the analog output from the geophones and record signals. The most common choice is a multichannel seismograph, which is specifically designed for seismic acquisition. Typically, one or two seismographs are connected to the geophone arrays (the number depends on the number of geophones used).

During data recording, the sampling rate affects the retrieved *f*. The sampling frequency (f_s) should be at least equal to twice the maximum *f* of the propagating signal. For surface wave analysis, a sampling interval of 2 ms (f_s = 500 Hz) is adequate for most situations. The recording time window must be long enough to record the entire surface wave train. A window of 2 seconds is usually sufficient for most arrays, but it is suggested to use longer windows when testing on soft sediments and/or longer arrays. Additionally, passive surveys require much longer acquisition times to ensure adequate acquisition of multi-directional ambient vibrations.

2.5. MASW Using Love Waves

Surface wave methods, such as SASW and MASW, are proven non-destructive geophysical techniques capable of generating accurate V_S profiles (Yong et al., 2013; Park et al., 2007; and Foti et al. 2017). Significant efforts have been devoted to the research and application of Rayleigh waves in MASW (MAS_RW). Although Love waves have been utilized in seismological studies for many years (e.g. Lay and Wallace, 1995), the application of Love waves to MASW (MAS_LW) has only recently gained traction (Yong et al., 2013). Two of the earliest known applications of Love waves for the characterization of V_S are by Mari (1984) and Song et al. (1989). More recent publications on MAS_LW include Safani et al. (2005), Eslick et al. (2007), Pei (2007), Xia et al. (2012), Yong et al. (2013), Yin et al. (2014), and Mahvelati and Coe (2017).

These research efforts indicate that Love waves are particularly well-suited for sites with sufficient stiffness contrast near the subsurface. Generally, Rayleigh waves can penetrate approximately 1.3-1.4 times deeper than Love waves with the same λ (Song et al., 1989). However, this applies when only considering fundamental mode behavior as both waves demonstrate similar penetration depths at higher modes (Yin et al., 2014). As outlined by Xia et al. (2012), Love wave inversion has the following advantages relative to traditional Rayleigh wave inversion:

1. The independence from V_P makes Love wave dispersion curves simpler than Rayleigh waves and reduces the non-uniqueness of the inversion process.
2. The dispersion images of Love-wave energy have a higher *SNR* and more focus than those generated from Rayleigh waves, which makes picking phase velocities easier and more accurate.
3. The inversion of Love wave dispersion curves is less dependent on initial models and more stable than Rayleigh waves.

However, due to a lack of research, it is unclear how changing variables such as the number of sensors, receiver geometry, site conditions, and source impact angle affect the accuracy of the MAS_LW results. Therefore, further research efforts must be undertaken to understand the full potential of Love waves in geophysical testing. This research study addresses one particular aspect of MASW with Love ways; that is, the role of impact angle on the generation of Love wave energy.

2.6. Simultaneous Generation of Rayleigh and Love Waves

Traditionally, MASW has been performed using solely the generation of Rayleigh waves despite the potential benefits offered by use of Love waves. If both Rayleigh and Love wave data are collected and analyzed, the uncertainty associated with the inversion process may be significantly reduced. However, Rayleigh and Love waves propagate most strongly in directions perpendicular to one another – Rayleigh waves in the vertical direction and Love waves in the horizontal direction. Rayleigh and Love waves have therefore been traditionally generated by vertical and horizontal strikes, respectively (Figure 2.4). Vertical wave propagation is measured by vertical geophones, and horizontal waves are measured by horizontal geophones. As a result, Rayleigh and

Love waves are recorded separately and twice as many tests must be conducted to obtain the data necessary for the analysis of both Rayleigh and Love waves. So, while MASW using both Rayleigh and Love waves may increase the accuracy of the velocity profile compared to single MASW, the time and effort of data collection is significantly increased and often impractical.

If Rayleigh and Love waves are generated and recorded simultaneously, the efficiency of the data acquisition process could be drastically improved. In return, $MAS_{RL}W$ would become a more appealing process due to the benefit of increased accuracy with minimal changes to analysis time and/or effort. Therefore, the topic of simultaneous generation is an area well worth investigating.

Unfortunately, there have been very few studies devoted to simultaneous generation of Rayleigh and Love waves for MASW. During the field analysis portion of one study by Dal Moro and Ferigo (2011), horizontal geophones were oriented parallel to the array in order to record the radial component of Rayleigh waves generated by a vertical strike. The dispersion curves for Rayleigh waves were picked by considering both the radial and vertical components. Love-wave velocity spectrum results were largely dominated by the fundamental mode. Dal Moro and Ferigo (2011) determined that the joint inversion of Rayleigh and Love waves is an extremely useful tool to clarify possible interpretive issues that may occur, although the joint analysis becomes less useful at the deepest layers. Furthermore, although the dispersion curves of the vertical and radial components of Rayleigh waves are the same, the energy distribution among different modes may differ significantly (Dal Moro & Ferigo, 2011).

Rayleigh and Love waves are generated most strongly by a purely vertical and purely horizontal strike, respectively. However, it is relatively common to use angled strike against an angled base plate to generate Love wave energy. The quantitative effects of impact angle on waveform data quality data and the optimal angle of impact are not well established in the literature for this configuration. A study by Hausler et al. (2018) examined the effectiveness of a multicomponent (three-sided) specialized seismic source (Galperin source) angled at 54.74°. The Galperin source was compared to a two-sided source angled at 45° and a traditional base plate (Figure 2.5).

The researchers noted that multicomponent acquisition enables a more complete observation of the seismic wavefield compared to a single-component source. Multicomponent sources can be used to generate both horizontally and vertically polarized shear waves. Sledgehammer strikes on both sources generated measurable signals for Rayleigh and Love waves. It was also determined that the sledgehammer impact angle on the source had a significant impact on the quality of data. To obtain the best data, the source should be struck normal to its face. The Galperin source allowed for fast multicomponent seismic data acquisition with equal source coupling for all three components without the need for changing or moving the source components (Hausler et al., 2018). This study and other studies on angled sources [e.g. Hardage et al., 2011; Schmelzbach et al., 2016; Gaiser, 2016] indicate that an angled source is capable of generating sufficient energy for surface wave testing with both Rayleigh and Love waves, though an optimal angle was not provided.

While these studies indicate that Rayleigh and Love waves may both be generated from an angled source, it is unclear whether Love waves can be recorded from the purely vertical impacts used to

generate Rayleigh waves. This research effort examines whether the dispersion image generated from a vertical impact can be effectively used to evaluate a V_S profile.

2.7. Summary

MASW presents a rapid, effective manner by which to estimate subsurface stiffness using either Rayleigh or Love waves. However, as noted in this chapter, there are some major limitations related to the uncertainty introduced in the data acquisition, post-processing, and inversion process. MASW using both Rayleigh and Love waves presents a way to mitigate some of the issues related to the uncertainty (e.g., joint inversion to reduce inversion non-uniqueness). However, Rayleigh and Love waves are typically collected using different sources and impact angles. Extracting Rayleigh and Love waves from a single impact would greatly reduce the data acquisition time and improve the efficiency of the $MAS_{RL}W$ process. Very little research has been performed on this topic of simultaneous generation, particularly with respect to how the impact should be angled from the ground surface to optimize the Rayleigh and Love waveforms. Therefore, further research is necessary to study this issue. To that effect, MASW testing was performed alongside other seismic geophysical testing at one site in southeastern Pennsylvania. V_S profiles were created using data from both independent and joint inversion of Rayleigh and Love waves generated using different impact angles and compared with the V_S profiles obtained from other seismic geophysical testing. Moreover, the acquired signals were compared with respect to *SNR*, spectral content, dispersion information, and inverted V_S profiles. This was also examined for the case of a purely vertical impact and the effectiveness with which it could generate useable Love waveforms for MASW.

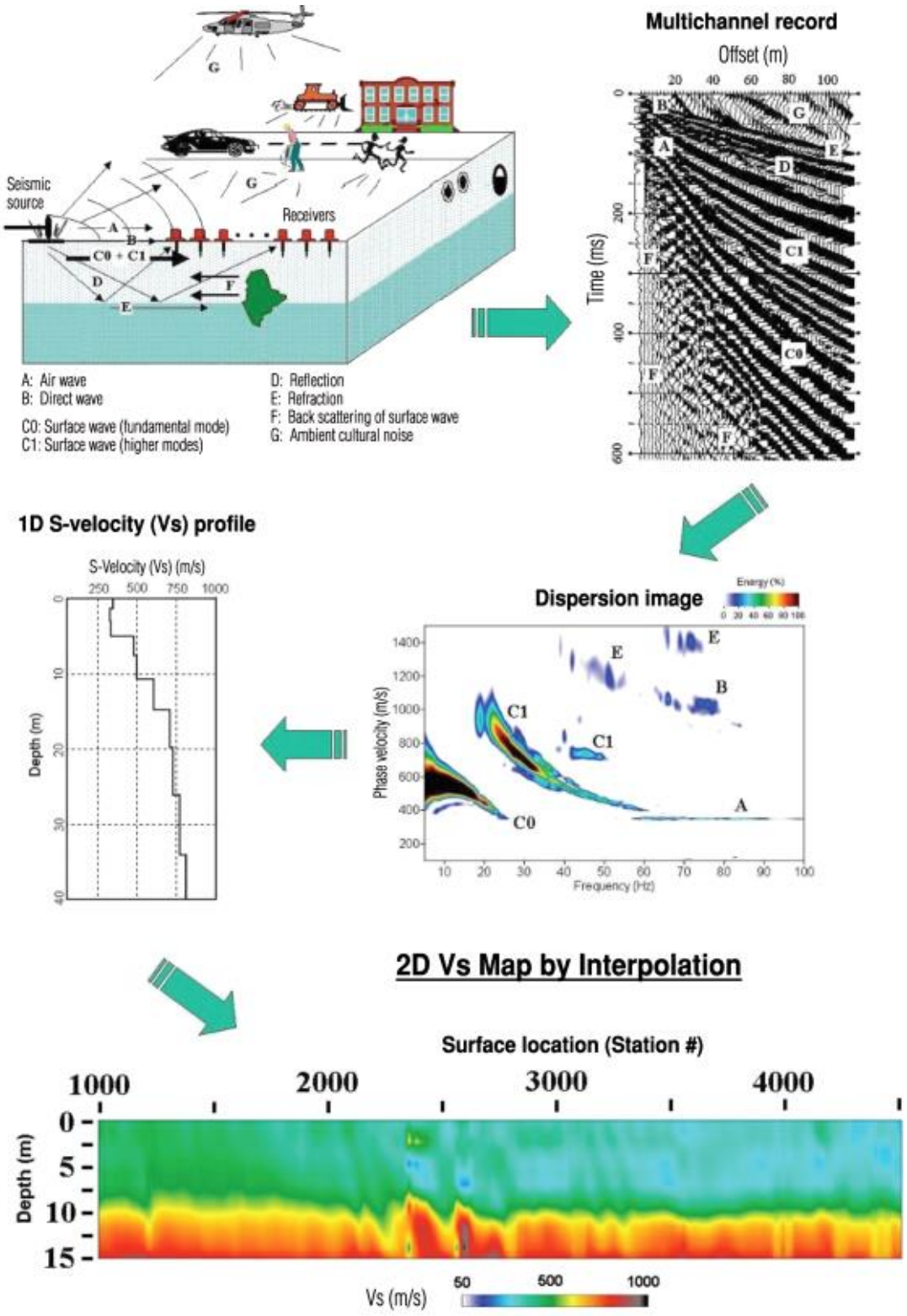

Figure 2.1. An illustration of the overall MASW procedure (Park et al., 2007).

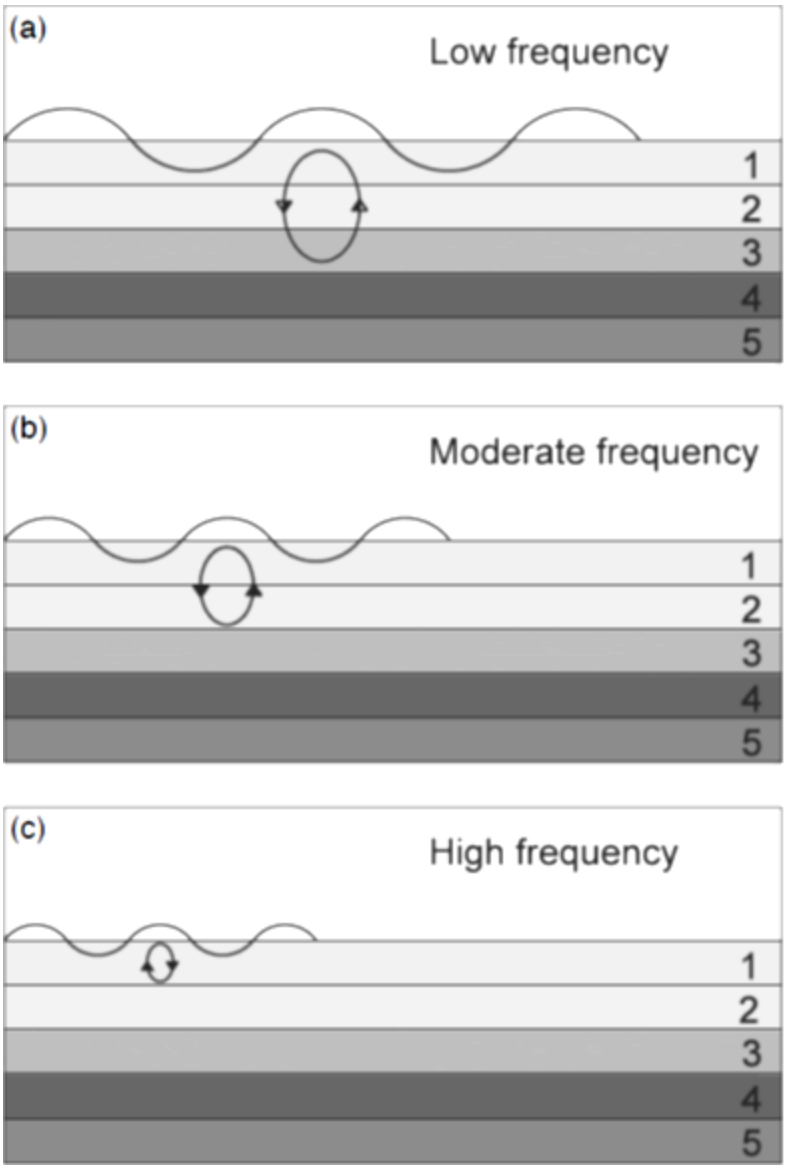

Figure 2.2. Low f (long λ) waves (a) penetrate deeper than waves of higher f (shorter λ) (b) and (c). (Ólafsdóttir, 2014).

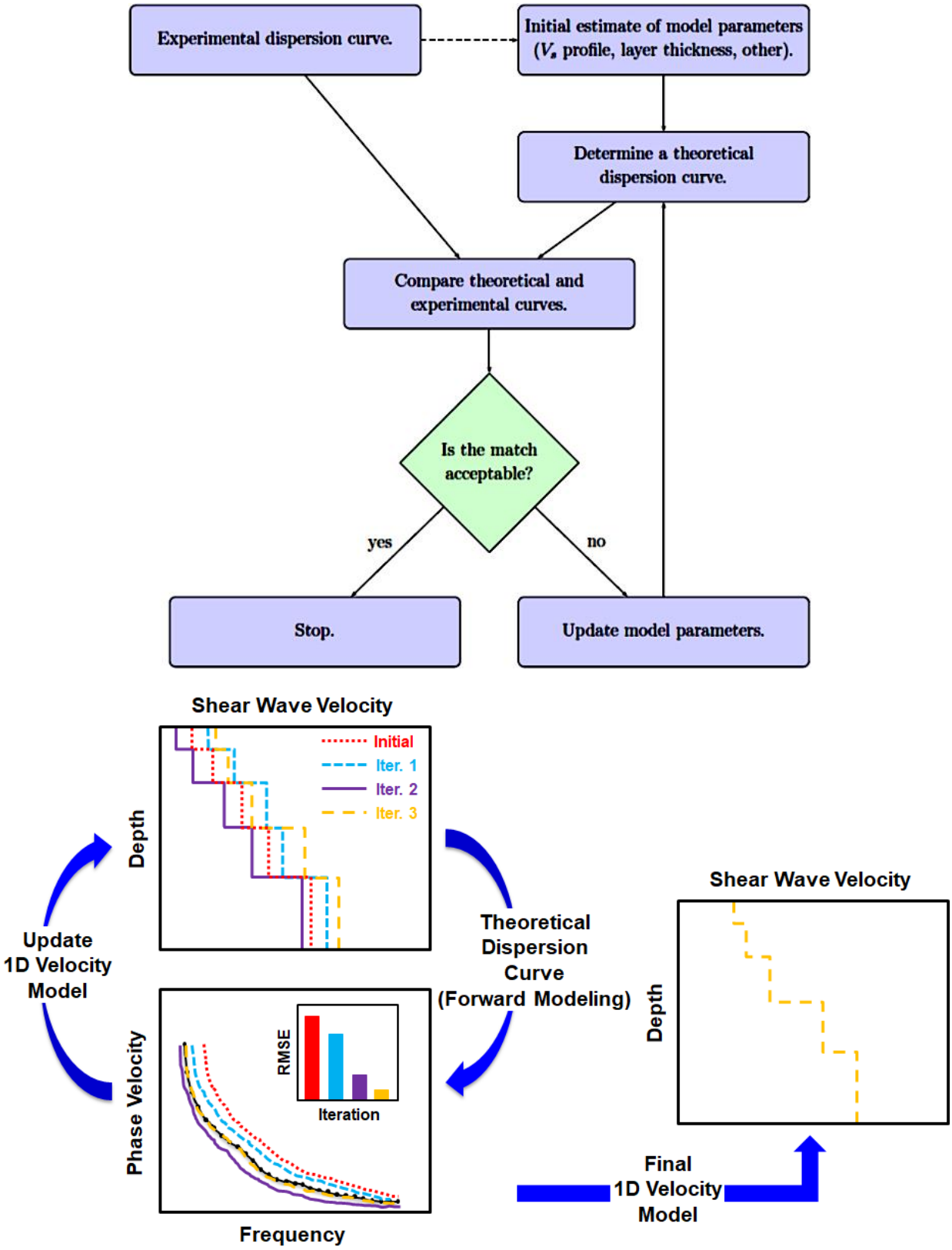

Figure 2.3. Flowchart and schematic of a typical local inversion algorithm (Olafsdottir, 2014).

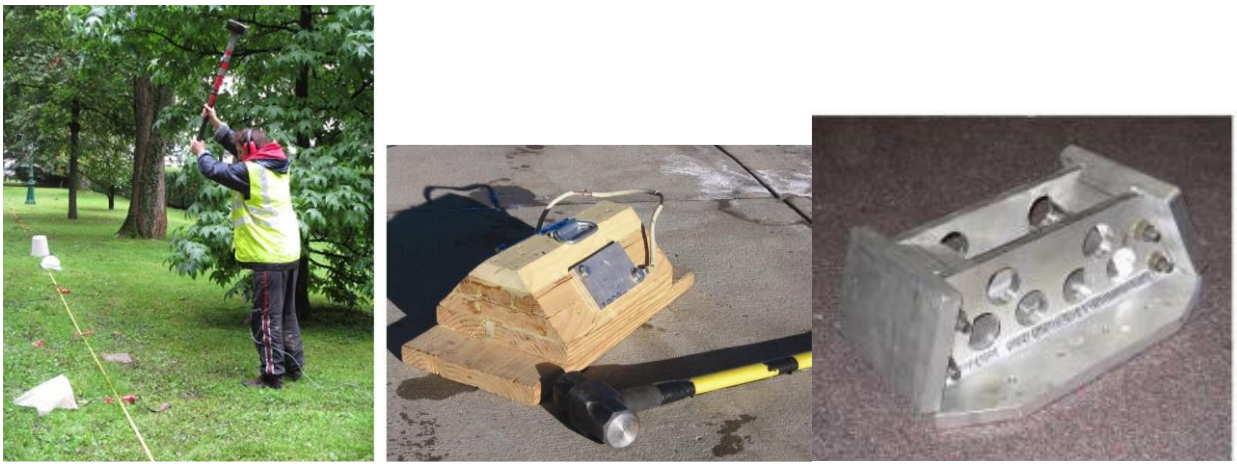

(a) **(b)** **(c)**

Figure 2.4. Surface wave sources: (a) vertical source for Rayleigh waves; (b) angled wooden source for Love waves; and (c) aluminum horizontal source for Love waves (Foti et al., 2017; Haines 2007).

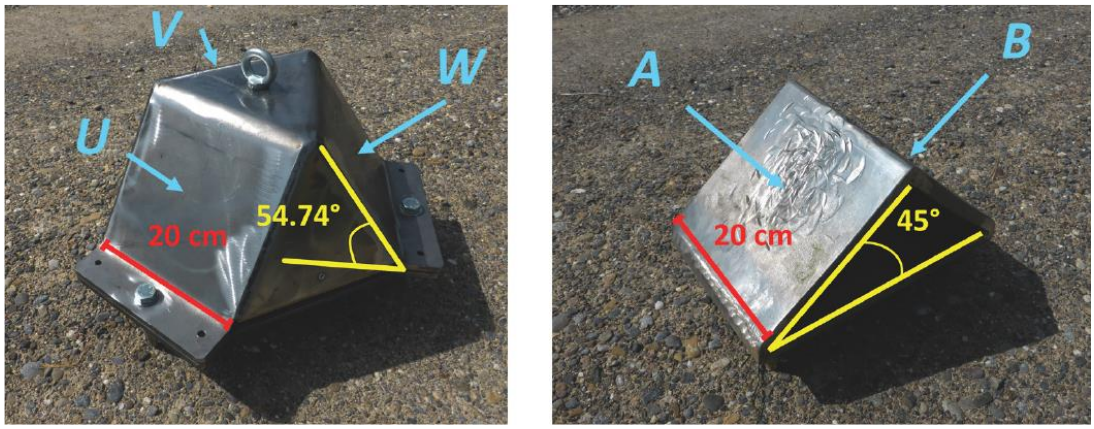

Figure 2.5. Galperin source and traditional angled base plate (Hausler et al., 2018).

3. DATA COLLECTION AND PROCESSING

For this project, field testing was performed at Temple University's Ambler campus by the research team. The following sections present the selected field site, testing procedures, and data post-processing used to generate results.

3.1. Test Site

The MASW field testing was performed at Temple University's Ambler campus, specifically at the Ambler baseball field (coded as TAB in field logs) (Figure 3.1). This site was selected to represent a "normally" dispersive profile (i.e., one that exhibits the typical increase in stiffness with depth). The site was also chosen due to the availability of ground truth information and V_S profiles from previous seismic downhole and refraction testing (for details see Mahvelati, 2019) (Figure 3.2).

The TAB site, which is located approximately 24 km north of the city center, is underlain by the Stockton Foundation. The Stockton Formation is composed primarily of medium to coarse grained sandstone, siltstone, and mudstone with shale interbeds. Ambient traffic was generally moderate at the site since it is located adjacent to Meetinghouse Road, a moderately used suburban road. However, testing was typically paused in response to the start and/or end of classes at the Temple University Ambler campus when vehicular traffic increased. The ground surface at TAB consisted of soft to medium-stiff unconsolidated sediments such as silts, sands, and clays. The site lacked gravely soils or obstructions which allowed for good ground coupling of the geophones using spikes.

3.2. Field Testing

Field testing for MASW generally followed recommended best practices as per Yong et al. (2013) and Foti et al. (2018). The following sections highlight the specifics of the array geometry, impact plates, and data collection filed procedures.

3.2.1 MASW Array Geometry

MASW testing was conducted using active surveys at the TAB site. A linear receiver array of 24 geophones was used to acquire the surface waveforms. Vertical-component geophones (4.5 Hz) were used for Rayleigh wave testing and horizontal-component geophones (10 Hz) for Love wave testing. Both Rayleigh and Love wave testing was conducted using three different receiver intervals (*dx*): 0.5 m, 1.0 m, and 1.5 m. This resulted in total array lengths of 11.5 m, 23.0 m, and 34.5 m, respectively. Sledgehammer impacts (also referred to as "shots" in geophysical terminology) were generated at offsets from one end of the array: -6dx, and -12dx. These source offsets (*SO*) were selected to avoid near and far-field effects as noted in Yoon and Rix (2009).

3.2.2 MASW Seismic Sources and Impact Plates

A 20 lb sledgehammer and a GISCO ESS-MINI accelerated weight drop (AWD) were used as seismic sources in this study (Figure 3.3). Impacts were performed on sources angled at 0°, 15°, 30°, 45°, and 90° from vertical. The 20 lb sledgehammer was only used to perform the 90°impacts since the AWD was incapable of that orientation. Variability in sledgehammer impacts was reduced by using the same hammer operator, incorporating periods of rest to prevent fatigue, and averaging the data from multiple hammer strikes. These efforts improved reproducibility and ensured that the findings were statistically meaningful. These precautions were not needed when using the AWD as the device is mechanical and produces consistent strikes. At each shot location, multiple hammer strikes (typically 4) were stacked in order to increase the *SNR* of the recorded waveforms.

The base plate used in MAS_RW testing was a 0.3 m x 0.3 m x 1.25 cm-thick aluminum plate. Three different base plates were constructed for MAS_LW testing. Each base plate consisted of a 15 cm x 15 cm x 2.5 cm-thick aluminum plate over a wooden base which was cut at angles of 15°, 30°, and 45°. Figure 3.4 shows impact plates of 15°, 30°, and 45°. A 90° source was used for Love wave testing that consisted of a 15.2 cm x 15.2 cm x 61 cm lumber post with galvanized caps on each end. The vertical side of the plate was struck to produce horizontal ground motions.

3.2.3 MASW Data Collection

A Geometrics Geode seismograph and a field laptop with the Geometrics Seismodule Controller Software (SCS) were used to acquire data. The surface waves were sampled at an interval of 0.125 ms for a total duration of 2.048 s (i.e. 16,384 samples). Initially, a trigger switch was attached to the sledgehammer to begin data recording once impact was made on the baseplate. However, this trigger proved inconsistent, so a geophone was planted adjacent to the baseplates as a triggering mechanism for data collection

3.2.4 Additional Seismic Geophysical Testing

Previous to MASW testing at the TAB site, seismic refraction and downhole tests were also performed to obtain ground truth information. Testing was performed at existing boreholes/monitoring wells at the TAB site. The results from seismic refraction and downhole tests were combined to generate a ground truth model of velocity (Figure 3.2) with which to compare the results of the $MAS_{RL}W$ testing. Details for this testing and analysis are provided in Mahvelati (2019).

3.3. Data Processing

The data collected during these field investigations were post-processed using custom scripts in the MATLAB computing environment, the Geometrics SeisImager/SW® software package, and the Geopsy open-source seismic processing software package. The recorded signals were evaluated for spectral content and relative energy using MATLAB. Subsequently, the dispersion images (also referred to as overtone images) were generated in SeisImager/SW® which uses the phase-shift method (Park et al., 1998) to convert the multichannel records in the time (t)-space (x) domain into the frequency (f)-phase velocity (C_f) domain. Once fundamental mode dispersion curves were selected from the overtone images, they were imported into the Geopsy software package where a GSM neighborhood inversion algorithm (Wathelet, 2008) was implemented to estimate the subsurface V_S profile. Additional details about each of these steps is provided in the following sections.

3.3.1 Spectral Content and Relative Energy

The acquired signals and corresponding dispersion images were examined for changes in energy and spectral content. Spectral content was examined by generating the power spectra from the raw signals using SeisImager/SW® and MATLAB. The shapes of the resulting power spectral density (PSD) plots were compared using peak values, dominant frequency (f_{dom}), and the shape factor (δ) as a proxy for signal bandwidth (Vanmarcke 1976; Kramer, 1996):

$$\delta = \sqrt{1 - \frac{\lambda_1^2}{\lambda_0 \lambda_2}} \qquad \text{(Equation 3.1)}$$

where λ_n is the nth spectral moment and can be computed as:

$$\lambda_n = \int_0^{\omega_N} G(\omega)\omega^n d\omega \qquad \text{(Equation 3.2)}$$

where ω is the angular frequency, ω_N is the Nyquist angular frequency, and $G(\omega)$ represents the PSD of the signal. Larger δ values correspond to larger signal bandwidths and δ always varies between 0 and 1 (Kramer, 1996). Additionally, energy levels were evaluated based on the "relative energy" concept introduced by Miller et al. (1986), where the summation of the squared Fourier amplitude spectrum (i.e., power spectrum) provides an estimate of the energy generated by an impact source and transferred into the underlying ground surface.

3.3.2 Signal to Noise Ratio (SNR)

SNR of the recorded waveforms were examined to evaluate the degree to which impact angle negatively affect the raw signals. *SNR* represents the quality of collected waveforms and is defined

as the ratio of the signal power to the noise power. When the signal amplitude (A_S) and noise amplitude (A_N) are measured, *SNR* can be calculated using:

$$SNR = 20 \log_{10}\left(\frac{A_S}{A_N}\right) \qquad \text{(Equation 3.3)}$$

where *SNR* is expressed in units of decibels (dB). In this study, *SNR* was determined for a given trace by comparing the maximum amplitude of the coherent signal within a shot window to a representative noise level recorded at the site of interest. In other words, all the maximum amplitudes extracted from the waveforms were divided by a constant amplitude representing the average noise threshold at the site. This representative noise level was estimated at each site based on data from several acquisitions at different offsets. The maximum amplitude of signals picked from the latter part of the recording duration (i.e., after the primary shot signal has completely propagated through the receiver array) were subsequently selected and averaged. The reason for this approach is that different records were influenced by different amounts and sources of background noise. Even though caution was used during field testing to collect data when background noise was minimized, these noise levels still fluctuated and could systematically bias the estimates of *SNR* if each trace were normalized by its own level of background noise.

3.3.3 Dispersion Information

For this research effort, the overtone images from MASW testing were used in two ways. First, they were examined to extract a fundamental mode dispersion curve for the site. To extract this curve, suggested points from the automatic algorithm embedded in the SeisImager/SW® software were cross-examined with theoretical dispersion curves computed for the ground truth model at the TAB site. The curve selection process was repeated for all the shot records of interest and multiple dispersion curves were extracted. Then, select subsets of dispersion curves were averaged together to create representative dispersion curves as described in Olafsdottir et al. (2018). The dispersion curve data points from Rayleigh and Love waves, regardless of their offset, source, or interval, were averaged and examined in a single figure. This process allowed for direct comparison of MAS_RW and MAS_LW dispersion curves. Next, the dispersion curves were analyzed based on an average according to base plate angle.

The overtone images were also evaluated directly and compared with each other by taking their difference. This allowed a review of the following issues: energy partitioning between the fundamental and higher modes, low-frequency fundamental-mode performance, high-frequency fundamental-mode performance, and uncertainty in fundamental mode dispersion curve interpretation.

3.3.4 Inversion

The dispersion curves generated in the previous step of data post-processing were used in the GSM implemented within the Geopsy software package to perform both independent inversion of Rayleigh and Love waves and joint inversion. This GSM uses an improved neighborhood algorithm developed by Wathelet (2008). Rather than starting from an initial "guess" of the subsurface V_S as in a local search method, this GSM defines a probability density distribution for each model parameter (i.e., V_S, V_P, ρ, t). This parameterization creates a range of potential models over which the global algorithm searches for the best model, using a randomly generated seed model for the starting point (Foti et al., 2017). This seed model is iteratively adjusted to identify the best model whose forward response fits the experimental dispersion information (obtained in the previous step).

The control parameters implemented in the neighborhood algorithm within Geopsy include: (1) the number of models chosen at random inside the parameter space at the beginning of the inversion (NS_0); (2) the number of models to generate at each iteration (NS); and (3) the number of best cells (with the lowest misfit) where the NS models are generated (NR). Selection of an appropriate parameterization must balance the need to explore a wide range of potential models with computation expense and the extent to which most models represent unrealistic subsurface conditions for the site of interest (Cox and Teague 2016). The inversion is more exploratory if the NS new samples are distributed on many cells (i.e., NR is high). The inversion is more restrictive if it optimizes more by limiting the NS new samples to the very few best cells (i.e, NR is low). Wathelet (2005) notes that generally better misfits are obtained with fewer iterations if NR is low, but the inversion is more trapped in local minima. Consequently, larger values for NR and NS can provide better final misfits at the expense of greater number of iterations and the associated computational costs.

For this study, the model was parameterized using the following criteria:

- P-wave Velocity (V_P): 6 layers (5 plus a halfspace) limited to V_P between 200 m/s to 8000 m/s. Bottom of layer was linked to the bottom of the layers defined for V_S.
- S-wave Velocity (V_S): 6 layers (5 plus a halfspace) limited to V_S between 150 m/s to 4000 m/s.
- Density (ρ): Single layer with fixed 2000 kg/m^3 value.
- Poisson's Ratio (ν): Single layer limited between 0.2 to 0.5.
- Inversion Tuning Parameters: NS_0 = 100; NS = 50000; NR = 100.

In order to evaluate the effectiveness of the inversion, a misfit function is defined, which represents how close an experimental dispersion curve is to the measured dispersion curve during the subsequent forward modeling. For this study, based on the information input into the inversion algorithm, this misfit function simplifies into a root-mean-square error (RMSE):

$$RMSE = \sqrt{(\frac{1}{N})\sum_{i=1}^{N}(C_i^T - C_i^M)^2} \qquad \text{(Equation 3.4)}$$

where C_i^T and C^M_i are the phase velocity at the *i*th frequency component for the theoretical and measured dispersion curves, and N is the total number of data points. V_S models were selected based on the lowest RMSE misfit within a tolerance of +1%. This allowed for some measure of the uncertainty involved in the global inversion process.

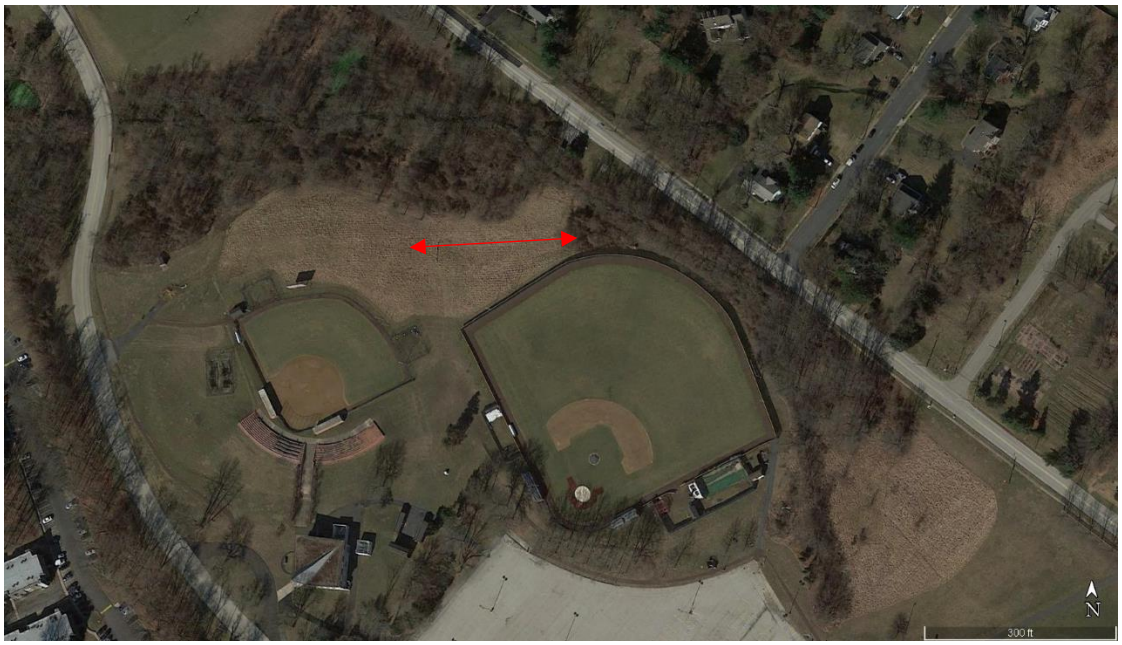

Figure 3.1. Temple Ambler campus site and survey line (Google Earth).

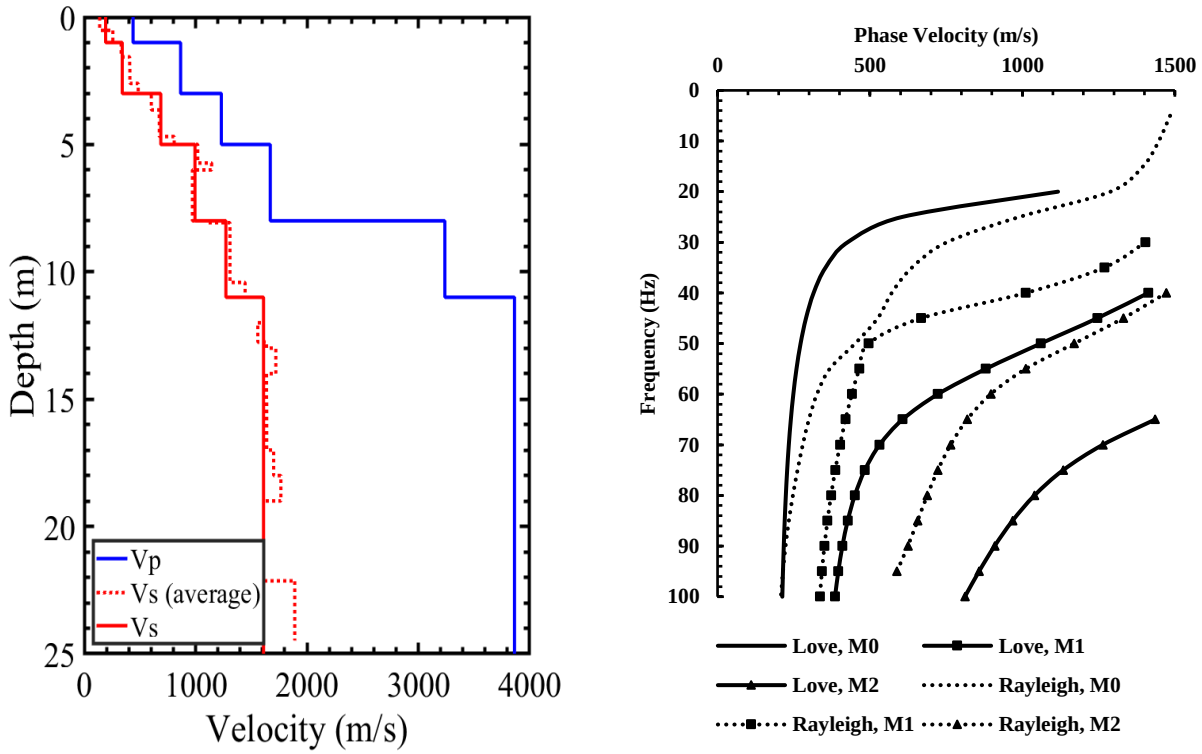

Figure 3.2. Ground truth model at TAB: (a) V_S and V_P profile; and (b) Rayleigh and Love wave dispersion curves (Mahvelati, 2019).

Figure 3.3. AWD positioned at impact angles of 15°, 30°, and 45° (Mahvelati, 2019).

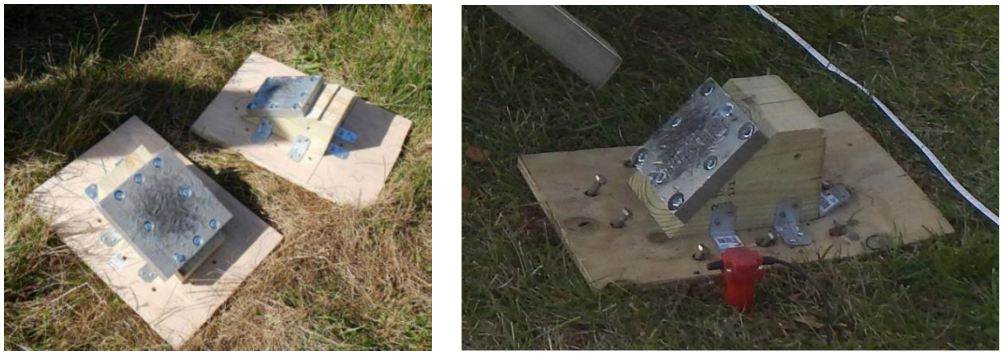

Figure 3.4. Custom impact sources for 15°, 30°, and 45° (Mahvelati, 2019).

4. Analysis of Results and Discussion

In order to understand the effect of base plate angle on the simultaneous generation of Rayleigh and Love waves, the frequency (*f*) content, relative energy, and signal-to-noise ratio (*SNR*) of the waveforms were examined. Shear wave velocity (V_S) profiles were also generated through independent and joint inversion of the acquired Rayleigh and Love waveforms. These results were generated for all testing performed at the site with both an accelerated weight drop (AWD) and 20 lb sledgehammer source and multiple source offsets (SO = -6*dx* and -12*dx*), receiver spacings (*dx* = 0.5 m, 1.0 m, and 1.5 m), and impact angles (0°, 15°, 30°, 45°, and 90°) as described in Chapter 3. The multiple SO and *dx* were used to ensure repeatability of the trends exhibited across impact angles. The results presented herein were developed in service of answering the following two research questions:

1. What is the optimal angle of impact for simultaneous generation of Rayleigh and Love wave generation?
2. How effective are vertical impacts for generating simultaneous Rayleigh and Love waves?

The following sections highlight the major findings of this study with respect to these research questions.

4.1. Frequency Content

The *f* present in a surface wave is an important parameter to ensure adequate coverage for development of a dispersion curve during MASW analysis. It was anticipated that changes to the impact angle would result in different performance with respect to *f*. For example, certain frequency bands may be more emphasized than others as the impact angle was varied from vertical to horizontal. This was initially examined by transforming the time-domain waveform signals into the *f* domain. The Fourier transform of a signal breaks down the entire signal into individual *f* components. The power spectrum [or power spectral density (PSD)], which similarly examines the relative power contribution of each *f* component, is computed by squaring the magnitude of a signal's Fourier amplitude spectrum, normalized by the number of *f* samples.

Figures 4.1 and 4.2 plot the normalized PSD of the collected waveforms as a function of *f* for the different SO, *dx*, and impact angles. Each sub-figure was normalized to the largest peak PSD within the plotted dataset. For Rayleigh wave data, the 90° orientation was not collected during field testing. A higher PSD indicates that a particular *f* component was more prevalent in the acquired waveform data, which should generally improve recognition of its corresponding phase velocity within the dispersion image. Therefore, the relative differences between curves in each sub-figure indicate how much the impact angle improved or degraded the power contributions of a particular *f* range and its presence in the corresponding dispersion image. Consequently, these normalized PSD plots were analyzed to examine differences in their relative shape and peak PSD values.

4.1.1 Rayleigh Waves

The Rayleigh wave power spectra remained generally consistent when observed across the various SO and *dx* used in this study. One of the first observations that can be made when comparing the normalized PSD plots is the relationship between impact angle and peak PSD. Impact angles of 0° and 15° produced the largest peak PSD values, while a 45° impact typically had the lowest peak values no matter the SO or *dx*. An outlier in this trend occurred at the -6*dx* and 0.5 m spacing, where the 45° impact produced a peak PSD value comparable to the other impact angles. The vertical polarization of Rayleigh waves explains the lower peak PSD values for the 45° impacts, which was 0.60 when averaged among the three offsets. This is a significant reduction compared to the 0° and 15° impacts (i.e., a 65.7% difference and a 58.8% difference, respectively).

When the peak normalized PSD values were averaged over both the -6*dx* and -12*dx* offsets, the 0° impact again produced the largest peak normalized PSD as would be expected for Rayleigh wave generation that tends to favor vertical strikes (i.e., 0° impacts). However, the average difference between the peak power of the 0° and 15° impacts (across all SO and *dx*) was less than 4.5%. Likewise, the difference between 15° and 30° impacts when averaged across SO and *dx* was approximately 10%. This implies that impacts at slightly less than vertical can still generate significant power in the dominant *f* band of the propagating wave. Moreover, the Rayleigh wave PSD seem to exhibit less overall sensitivity and scatter with respect to the impact angle. The switch from a 30° impact to a 45° impact proves to be the most detrimental to peak PSD based on the results of Figure 4.1.

Changes in impact angle may have a significant impact on the overall shape of the PSD plot, which can manifest as shifts in the dominant *f* present in a waveform and the overall bandwidth. Therefore, dominant frequency (f_{dom}) and signal bandwidth are also important factors to consider for frequency content analysis. The f_{dom} is the frequency that carries the most energy in the spectrum. Bandwidth is the difference between the upper and lower frequency in a continuous band of frequencies. It is typically found by examining the PSD plot and determining the first and last frequency associated with a power spectral density equal to half the peak value (Kramer 1996). However, this definition causes the measured bandwidth to be highly affected by localized variations in the amplitude of the power spectra. In this study the shape factor (δ) as defined by Vanmarcke (1976) was used as a measurement of signal bandwidth as noted in Chapter 3.

Based on the results in Figure 4.1, the f_{dom} for the 0° impact was generally the highest of all the impacts, regardless of the source offset and receiver spacing (Table 4.1). This implies that by angling the impact away from vertical, the peak PSD values shift to lower frequencies. However, these changes were a rather small effect. On average, the difference between maximum f_{dom} (0° impact) and minimum f_{dom} (typically 45° impact) was 7.7%. The results for δ pointed towards an overall increase in bandwidth as the angle was shifted away from 0° towards more horizontal (Table 3.2). For example, δ increased on average by more than 4.5% at 15°, 30°, and 45° impact angles when compared to 0° impacts. This implies that the shift in the f_{dom} towards lower

frequencies at more horizontal impacts was also accompanied by an overall broader shape for the PSD plot. Consequently, although the peak PSD value decreased with the 15°, 30°, and 45° impacts as a result of the energy partitioning into both vertical and horizontal components, there was an overall shift towards increased participation from a broader range of frequency bands.

4.1.2 Love Waves

The Love waveforms were analyzed in the same manner as the Rayleigh waveforms. For Love wave generation, the purely horizontal (90°) impact actually proved to generate the smallest peak normalized PSD value. This was related to the seismic source used for the 90° impact (20 lb sledgehammer), which generates substantially less energy than an AWD. The 0° impact generated the second lowest peak normalized PSD. This result also makes sense given that a purely vertical impact will primarily generate vertically-polarized wave energy. Nevertheless, an examination of Figure 4.2 highlights that even a purely vertical impact will generate normalized power spectra within approximately one half the peak normalized PSD from more favorable impact orientations. Moreover, use of an AWD will allow this 0° impact to compare with a purely horizontal (90°) impact with a much smaller 20 lb sledgehammer seismic source.

The effectiveness of generating both Rayleigh and Love waves with a purely vertical strike (i.e. 0°) was also examined with regard to PSD. As was expected, the 0° impact produced the highest average peak PSD values for Rayleigh waves. However, for Love waves the 0° impact performed second worst, behind the 90° impact which used the significantly less powerful sledgehammer source. For Love waves, the 0° impact produced an average peak PSD value of 0.62 when averaged across all SO and *dx*. This value was within approximately 40% of the highest average peak PSD value. Consequently, although a 0° impact will produce significantly less powerful Love waves compared to an ideal strike, it may still be able to generate usable data for MAS_LW analysis.

Additional examination of the PSD in Figure 4.2 highlights that the 30° impacts unexpectedly generated the largest peak normalized PSD values in nearly every case. The 15° impact angle generated the highest peak normalized PSD for the closest source offset and receiver spacing and was generally within a few percentage points of the 30° impact angle. Consequently, when the peak normalized PSD values were averaged across the different offsets and receiver spacings, the 15° impact angle actually performed best for Love wave generation, with the 30° impact angle on average exhibiting only a 1.5% smaller peak normalized PSD. These results suggest that Love wave generation was more robust at less than optimal impact angles (i.e., 0°, 15°, and 30°).

The 45° angle of impact did not perform as well as predicted for Love wave generation in terms of peak power. These results are somewhat surprising, as Love waves tend to favor more horizontal impacts and the 45° impact had the largest horizontal component in the impact force vector compared to the flatter angles of 15° and 30°. The lower-than-expected PSD for the 45° impact may have been due to issues with ground coupling and/or general wear and damage to the source as testing progressed. For example, as the impact angle approached closer to horizontal with such

a large AWD source, the larger horizontal component of the impact force vector may have caused the base plate to slide along the top of the ground surface. More intermediate angles, such as 15° and 30°, contained enough vertical force during impact to "wedge" the base plate in place and actually couple the horizontal wave energy to the ground better.

As with the Rayleigh wave results, the Love wave PSD were examined for changes in shape and f_{dom}. The average f_{dom} varied similarly with impact angle compared to Rayleigh waves. As with the Rayleigh wave results, the shift away from the "ideal" impact angle (in this case from 90° towards more vertical impacts) led to an average decrease in the predominant frequency of similar magnitudes (Table 3.3). However, the trend was practically (though not technically) reversed for Love wave impacts relative to Rayleigh waves with respect to the bandwidth proxy selected for this study (i.e., δ). The Love wave PSD exhibited an increase in δ as the impact angle increased from completely vertical (0°). However, a completely vertical impact is the least optimal orientation for the seismic source when trying to generate horizontally-polarized Love waves. Consequently, when viewed as a trend from most favorable angle for Love wave generation (90°) to least favorable (0°), the δ tended to decrease, which implies a narrower bandwidth. This signifies that less than optimal impact angles for Love waves tend to "focus" their energy into a narrower frequency band shifted towards lower frequencies. The corresponding "loss" of high-frequency content may negatively impact the predictions of the V_S structure in the immediate near surface (e.g., upper 1 m to 2 m).

4.2. Relative Energy

It should be noted that peak normalized PSD does not directly measure the total wave energy, which is based on the entire waveform rather than a single "spike" in the PSD plot. Therefore, a more comprehensive parameter must also be examined to better analyze the effect of impact angle on the energy transferred into the subsurface. The summation of the squared Fourier amplitude spectrum (i.e. power spectrum) provides an estimate of the "relative energy" generated by an impact source based on the efforts of Miller et al. (1986).

Typically, higher relative energy translates to larger *SNR* and clearer dispersion curves, which can improve the accuracy of V_S profiles. Relative energy levels were examined as a function of impact angle to analyze how well a particular orientation transferred impact energy into the subsurface. The results of the relative energy analysis should compare favorably to the conclusions drawn from the peak normalized PSD analysis, though there may be some subtle difference introduced by the scale of the two parameters. Figures 4.3 and 4.4 plot the normalized relative energy as a function of array configuration (i.e. impact angle, SO, *dx*, and wave type). In each sub-figure, a normalized relative energy level of 1.0 indicates the highest energy when compared to the rest of the configurations.

4.2.1 Rayleigh Waves

The Rayleigh wave relative energy results in Figure 4.3 reinforced many of the same trends noted in the PSD results in Figure 4.1. For example, the 0°, 15°, and 30° impacts produced similar relative energy levels for both the -6*dx* and -12*dx* offsets. Generally, the 15° impact produced the highest average relative energy over the three *dx* values (1.5 m, 1.0 m, and 0.5 m) and both SO (-6*dx* and -12*dx*). At -12*dx*, the 0° impact produced the highest average energy over the receiver spacings. When the relative energy from -6*dx* and -12*dx* were averaged together, the 15° impact produced the highest normalized energy. However, the difference between normalized energy from the 0° and 15° impacts was just 1.6%. The weakest impacts for Rayleigh waves occurred at the 45° impact angle. At -6*dx*, the average relative energy for a 45° impact was 0.65. At -12*dx*, the average relative energy for a 45° impact was 0.48. The energy generated by a 45° impact for Rayleigh waves was 53.8% lower than a 15° impact. These results align well with the previous analysis of the PSD that seemed to point to modest sensitivity of impact angle for Rayleigh waves until an angle of 45° is reached.

4.2.2 Love Waves

For Love waves, the 30° impact produced the highest relative energy over both the -6*dx* and the -12*dx* offsets. The second-best impact angle for Love wave generation was 15° based on the normalized relative energy values. The difference between the energy generated by the 15° and 30° impacts was 11.8%, indicating that relatively vertical impacts can generate useful Love wave energy. As with the Rayleigh wave data, these results corroborate the PSD analysis based on peak values. However, there were some minor discrepancies. For example, the 45° impact at -6*dx* performed better in terms of normalized relative energy when compared to the normalized PSD. For the 1.5 m and 0.5 m *dx* values, the 45° impact produced a normalized relative energy of 0.92 and 1.0, respectively. However, the average relative energy at -6*dx* was again reduced by a significant outlier at the 1.0 m spacing.

The 90° impact generated the least energy due to the reduced power of the 20-lb sledgehammer compared to the AWD. The 0° impact performed second worst in terms of relative energy. To examine the effectiveness of generating both Rayleigh and Love waves using a vertical impact, the energy generated by a vertical strike was compared to the energy generated at an ideal angle. As was predicted and shown in the PSD analysis, the energy generated by a 0° strike was much lower for Love waves. The 0° strike generated 56.8% less energy than the most powerful strike. Nevertheless, the 0° impact results in Figure 4.4 indicate that a purely vertical impact with an AWD is capable of transferring as much energy into the ground as a 20 lb sledgehammer impacting a base plate at the most ideal angle (90°).

The 15° impact produced the highest normalized energy for Rayleigh waves over both the -6*dx* and -12*dx* offset. However, this average normalized energy was only 1.6% greater than the energy generated by a 0° impact. For Love waves, the 30° impact produced the greatest normalized energy

over both offsets. The 30° impact produced, on average, 11.8% more energy than the second-best impact angle, which was a 15° impact. The 30° impact also produced strong Rayleigh waves; the 30° impact was just 4.8% less powerful than the optimal 15° impact for Rayleigh waves. Therefore, based on relative energy, it appears that the 15° and 30° impacts produce similar results for the simultaneous generation of Rayleigh and Love waves. It should be noted, however, that higher relative energies do not necessarily translate to more clear and accurate dispersion images. While the 90° impact did not produce large peak energy for Love waves, the shape of the power spectra compared favorably indicating sufficient *f* coverage for the development of a useable dispersion image.

4.3. Signal-to-Noise Ratio (*SNR*)

As noted in Chapter 3, *SNR* was determined for the acquired waveforms by comparing the maximum amplitude of the coherent signal to a representative noise level (i.e. the average noise threshold at the site). The purpose of this analysis was to determine if differences in relative energy led to changes in *SNR*. Figures 4.5 and 4.6 plot *SNR* as a function of channel number along the receiver array, where the channel numbers increase with distance away from the source.

4.3.1 Rayleigh Waves

The plots of *SNR* for Rayleigh waves show that the *SNR* of the 45° impact was consistently the lowest out of the four impact angles. The highest *SNR* for Rayleigh waves was at the 15° impact, both for -6*dx* and -12*dx*. These results mirrored the observations in the PSD and relative energy analyses. When averaged across the all channels, the *SNR* value for a 15° impact was 9.8% larger than the *SNR* for the 45° impact. At distances closer to the source, the *SNR* ratio for the 45° impact was closest to the *SNR* of the other impact angles. The difference in *SNR* was exacerbated by increasing distance from the source. This trend indicates that for Rayleigh waves, the effect of impact angle on *SNR* becomes more apparent at greater distances. Note, for example, in Figure 4.5 how many of the *SNR* curves diverge more at the farther channels of the arrays. For *dx* of 1.5 m and 1.0 m, the *SNR* trend decreased with distance from the source. However, for *dx* of 0.5 m, the *SNR* increased with distance from the source. This discrepancy is likely due to the fact that the array length for *dx* = 0.5 m is short, at 12 m. Near-field effects may have degraded the *SNR* at the closer receivers.

4.3.2 Love Waves

The Love wave *SNR* was lowest for the 45° and 90° impacts, which was expected based on the previous results for *f* and relative energy. The *SNR* for the 90° impact was 7.1% lower than the highest average *SNR*, which was at the 30° angle. The lower-than-expected *SNR* for the 90° impact is caused by the smaller impact source used for testing at that angle. The 20-lb sledgehammer

generated significantly less power than the AWD, and less power generally equates to a lower *SNR*. As explained previously for the PSD and relative energy results, the low *SNR* for the 45° impacts may be attributed to issues with coupling between the impact source and base plate. This in turn can be attributed to two main sources: (1) relative slippage between the base plate and the ground surface; and (2) wear and damage of the base plate.

When the *SNR* for Love waves were averaged, both for -6*dx*, -12*dx*, and overall, the highest *SNR* occurred for the 30° impacts. The *SNR* at 30° was 7.5% higher than the lowest overall *SNR*, which was at 45°. Consequently, this optimal angle for *SNR* is lower than a hypothesized optimal angle of 45°.

Based on the percent differences between the maximum and minimum *SNR* values for both Rayleigh and Love waves, it appears that Love wave *SNR* is less affected by impact angle than Rayleigh waves. Nevertheless, the differences in minimum and maximum *SNR* were small. The optimal impact angle for generating the highest *SNR* was 15° for Rayleigh waves and 30° for Love waves. However, it should be noted that a higher *SNR* does not always translate to a higher quality dispersion image as discussed in the next section.

4.4. Effects on Dispersion Information

The dispersion curve is a critical component of the MASW procedure, so the effect of base plate angle on dispersion information should be examined. Though qualitative in nature, an analysis of the quality of the dispersion image can highlight any potential improvements in survey resolution and depth of investigation based on the potential to extract an accurate dispersion image over a wide *f* range. Figures 4.7 and 4.8 present the differences between overtone images generated by various impact angles at different offsets and *dx*. Each dispersion image was compared to the "optimal" dispersion image (replicated as the top sub-figure) based on impact angle (i.e. 0° for Rayleigh and 90° for Love). The blue and red color scheme represents a negative or positive difference in normalized amplitude, respectively. If more information is available from the optimal dispersion curve (i.e. 0 or 90°), red is present; if more information is available from the compared dispersion curve, blue is present.

4.4.1 Rayleigh Waves

For Rayleigh waves, the 0° impact produced the best dispersion curves in terms of clarity and fundamental mode identification. This conclusion follows the results of the PSD, relative energy, and *SNR* analysis, where a 0° and 15° impact generated the most power, transferred the most energy, and exhibited the best *SNR*. However, the quality of the Rayleigh wave dispersion curves was generally poor, even for the 0° impact angle. It was often difficult to identify an obvious and continuous fundamental mode dispersion curve in the overtone images even at an optimal impact

angle. This suggests that the TAB site exhibits a pattern of modal excitation that causes modal-mixing during surface wave propagation. Moreover, the use of angled impacts tended to intensify this effect. For example, the blue sections of the bottom sub-figures along the areas where a fundamental mode can be extracted indicate decreased normalized amplitude (i.e., decreased fundamental-mode participation during surface wave propagation). This indicates that the effect of an increase in impact angle from vertical is higher modal participation in the overtone image and more difficulty in selecting a fundamental-mode dispersion curve. There was generally little difference between the -6*dx* and -12*dx* offsets for Rayleigh wave overtone images. However, the 1.0 m receiver spacing tended to produce clearer dispersion curves, particularly at higher frequencies.

The 15° impact generally compared favorably to the 0° impact overtone images, particularly in the upper frequency range. The largest differences occurred below approximately 35 Hz. This trend may be due to noise that manifests as error during the phase-shift method. At the lowest end of the frequency range, the coherent signal competes with noise, which when processed into the overtone image yields incoherent amplitude information and large scatter in the dispersion information. Fundamental-mode identification suffered somewhat, but otherwise compared favorably between the 0° and 15° impacts above this frequency. The 30° impact also produced reasonably clear dispersion curves comparable to the 15° impacts. This is not completely surprising considering the energy generated by the 30° impact and the reasonably high *SNR*.

4.4.2 Love Waves

The 90° impact produced the clearest dispersion curves for Love waves. This outcome is expected given what is known about ideal Love wave generation but does not follow the trend of the power and *SNR* analysis. The fact that a 90° impact with a 20-lb sledgehammer could produce significantly less energy than other impacts and yet still generate the clearest overtone images shows that power does not necessarily equate to a quality dispersion curve. The 90° impact produced a strong fundamental mode over a wide range of frequencies.

Overall, the quality of the Love wave overtone images was excellent, and the fundamental-mode for Love wave propagation was significantly easier to identify than for the Rayleigh wave overtones. This indicates that the TAB site is one where Love wave propagation is less complex and less subject to significant modal-mixing. Arrays with the various *dx* produced dispersion curves of similar quality. However, higher modes became clearer as *dx* was increased. In general, higher modes were easier to identify through Love wave dispersion images than Rayleigh wave dispersion images.

In line with the conclusions drawn from the power and *SNR* analysis, the 45° and 30° impacts again performed well. Despite lower energy and *SNR*, the 45° impact performed second-best after the 90° impact. The largest differences in the overtone images for these impact angles and the 90° impact occurred at very low and very high *f*. As with the Rayleigh wave overtone images, this

discrepancy may be a result of noise manifesting as error. Despite the differences at high and low frequencies, a fundamental mode could still be identified that compared favorably to the optimal dispersion curve. Interestingly the 15° and 0° impacts also produced dispersion curves from which a similar fundamental mode could be identified, although there was significantly more variation throughout the entire overtone image for each of these impact angles.

For each impact angle, differences between the 90° and other overtones became apparent in the 40-60 Hz range. In this range, the overtone images of other impact angles performed worse in terms of fundamental-mode identification. The discrepancy became more distinct as the impact angle moved closer to 0°. While the differences between the 0° and the 90° overtone images were obvious, reasonably accurate dispersion curves were still able to be obtained from the 0° overtone images (Figure 4.9). Both fundamental and higher modes could be picked from the dispersion image. This result indicates that vertical strikes may be reasonably effective for generating Love waves, which could significantly improve acquisition times and increase the accuracy of the final V_S profile.

4.5. Shear Wave Velocity (V_S) Profiles

A series of V_S profiles was generated for both Rayleigh and Love wave data using the improved neighborhood inversion algorithm proposed by Wathelet (2008) and implemented in the Geopsy software package. The inversion was performed independently as well as jointly, for a total of three subsurface V_S profile estimates. The inversion parameterization was described in Chapter 3.

Figures 4.10a – 4.12a show V_S profiles for each impact angle of the Rayleigh and Love wave data collection. The solid line of each V_S profile represents the solution that best fits the dispersion curve obtained from field data. The dashed lines on either side of the solid line represent the uncertainty for the best fit solution. These dashed lines indicate comparable V_S profiles within a pre-specified limit of uncertainty (i.e., within 1% of the lowest misfit value). Dashed lines that are very close to the solid line would indicate that there is little velocity variability and/or uncertainty within those limits.

Figures 4.10b – 4.12b also present the associated misfit between the predicted V_S and the ground truth V_S (i.e., Equation 3.4 applied to differences between predicted V_S values instead of dispersion curves). These plots reflect how difference there is between the inverted and ground truth V_S estimates as a function of depth. A lower RMSE misfit indicates less error and vice-versa. Additionally, the rate of change in the RMSE plot indicates whether the velocity layer at that depth is improving the overall prediction or adding to the error. For example, when the RMSE decreases with depth, the inverted V_S profile is more accurately predicting the ground truth V_S. The intersection points with the x-axis in Figures 4.10b – 4.12b represents the global overall RMSE for the V_S profile (i.e. how accurate the entire profile is on average across the entire depth). For this research effort, seismic refraction and downhole testing were used to obtain ground truth information at the TAB site.

4.5.1 Rayleigh Waves

For Rayleigh waves, the inverted V_S profile generated by all impacts were practically identical for the upper 1.5 m of the site and exhibited the same RMSE between the predicted V_S and ground truth V_S. Beyond that depth the 45° results start to perform the worst compared to the other impact angles, though the difference is relatively modest. However, even the better-fitting V_S profiles varied significantly from the ground truth model through most of the profile, highlighting the issues faced at this site with MAS_RW.

While each impact angle performed similarly up to a depth of approximately 5 m, the 45° impact compared most favorably to the ground truth model at depths greater than 7 m. Because the 45° impact performed better at depth, it should be considered the best V_S profile compared to the ground truth model. This is indicated by the lowest overall RMSE between the 45° impact inverted model and ground truth. In fact, the global RMSE for the 45° impact angle when computed across all depths is approximately half the next smallest RMSE (0° impact).

Rayleigh wave V_S profiles had significant uncertainty (i.e. space between the dashed lines) at deeper strata. Uncertainty tended to increase as the impact angle approached horizontal. By far, the most uncertainty in the inverted V_S profile corresponded to the 45° impact. However, even the 0° impact angle suffered increased uncertainty at depth. It should be noted that although the 45° V_S profile appears to be close to the ground truth profile at depths greater than 7 m, the very high uncertainty of the 45° inversion prevents it from being considered an accurate V_S profile. The 30° impact actually appears to have the lowest V_S uncertainty at depth. This result may be due to the source orientation or stronger source-ground coupling that allowed more energy from the AWD impact to be generated into the subsurface. Consequently, when considering both RMSE and amount of uncertainty present in the inverted V_S profile, the superior Rayleigh inversion model appears to be the one generated from waveforms generated by a 0° impact (as would theoretically be expected).

Higher uncertainty at deeper strata can be explained by a lack of low-frequency energy in the surface wave. Lower *f* are required to accurately image deep strata, so if an impact angle is not able to generate *f* in such a range, the uncertainty at depth increases. This uncertainty is manifest in the V_S profile as a wider range of potentially viable inversion models. Greater uncertainty as the impact angle approached 45° indicates moving the impact angle towards horizontal negatively impacts low-frequency generation for Rayleigh waves. This appears to contradict the PSD results that pointed to a shift in low frequency response as the angle was made more horizontal. However, an examination of the relative energy quickly highlights that, though the predominant frequency may have shifted to a lower value/range, the overall energy transferred into the subsurface was drastically reduced for the 45° impact. This can consequently explain the increased inversion uncertainty at depth relative to the other impact angles.

4.5.2 Love Waves

In general, V_S profiles generated from Love wave data compared more favorably to the ground truth model than Rayleigh wave profiles. This was evident based on the lower overall RMSE values when taking the entire depth profile into account as well as the reduced inversion uncertainty present in the results of Figure 4.11. At the near surface (i.e. less than 3 m) Rayleigh wave V_S profiles tended to match ground truth information better than Love wave profiles. However, at intermediate depth (i.e. between 4 and 10 m), Love wave profiles showed improvements over Rayleigh profiles.

For Love waves, the 90° and 45° impacts generated the best-fit profiles. These impact angles also had the lowest uncertainty. While the 90° and 45° impacts performed best compared to the ground truth model, the other three impact angles produced reasonably similar V_S profiles. There was no significant difference between the impact angles at depths less than 3.5 m, but uncertainty in the inversion results increased as the impact angle approached vertical. This inversion uncertainty was notably less than uncertainty in the Rayleigh wave inversion, even for the worst-performing impact angles (i.e. 0° and 15°). As with the Rayleigh wave profiles, the trend of increased uncertainty with depth can be explained by a lack of low-frequency waves necessary to accurately image deeper strata. The accuracy of the Love wave V_S profiles may have been improved by using a more powerful strike for the 90° impacts and improving the ground coupling and durability of the 45° source.

For Love waves, the 30° impact performed reasonably well. At depths greater than 8 m, the 30° impact performed very similarly to the 45 and 90° impacts. The most notable difference between the 30° impact and the more horizontal impacts occurred at 5 m where the 30° angle underpredicted V_S. Uncertainty in the 30° inversion was also similar to the 90° and 45° inversions, although uncertainty increased at depths greater than 10 m. Although the 0° and 15° impacts performed moderately well at depths up to approximately 5 m, uncertainty increased significantly at greater depths. Still, the Love wave V_S profiles seemed to be less dependent on impact angle than Rayleigh waves with less overall scatter between the V_S predictions from different impact angles. Consequently, selection of an optimal impact angle may be able to be guided more explicitly by Rayleigh wave generation at this site given the sensitivity to impact angle and poor overall performance of Rayleigh waves due to modal-mixing and higher-mode participation.

4.5.3 Joint Inversion

Joint inversion of Rayleigh and Love waves was also performed to elucidate any further constraints on selection of the optimal impact angle. Figure 4.12 shows the results of joint inversion. Joint inversion seemed to improve the accuracy of V_S profiles relative to the ground truth model by combining the Rayleigh wave accuracy at shallow and deep layers with the Love wave accuracy at intermediate-depth layers. During joint inversion, uncertainty was likely reduced by the additional constraints introduced by utilizing both Rayleigh and Love wave data. Furthermore, the

joint inversion may have benefited from the higher-quality data offered by Love waves. In particular, joint inversion appears to have significantly less uncertainty as depth increased. Joint inversion also more closely aligned the V_S profiles of each impact angle, resulting in less overall scatter between the profiles. For example, while there were significant differences between the 0° and 45° Rayleigh wave profiles, the V_S profiles of these two impact angles performed similarly after joint inversion. After joint inversion, the 30° profile appears to have the best fit and lowest uncertainty though this profile was still appreciably different than the ground truth model.

4.5.4 Comparisons Between Inversion Results

The large differences between the MASW and ground truth V_S profiles for both Rayleigh and Love waves can potentially be explained by inherent differences in the seismic geophysical testing procedures used at the TAB site. While the boreholes used for downhole testing were close to the MASW site, they were not in the exact location. The subsurface may experience significant changes over a relatively small area. These differences could explain discrepancies between the inverted V_S profiles and ground truth. Likewise, the seismic refraction results were converted into a 1-dimensional V_S profile from a 2-dimenstional profile.

Compared to Rayleigh waves, Love waves performed slightly worse at the immediate near surface (i.e. above 1 m). Love waves performed better than Rayleigh waves for approximately 4 m through 11 m. In this range, the RMSE error was less for Love waves although the variability between impact angles was greater. The Love wave profiles exhibit slightly better RMSE at greater depths, but the 0° and 15° results were comparable to Rayleigh waves. For Love waves, the 90° impact performed best overall (with 45° not far behind), while the 15° impact displayed the highest RMSE. Interestingly, the 45° impact performed significantly better for Rayleigh waves than for Love waves. The accuracy of Love wave profiles seemed to be less sensitive to changes in impact angle.

The joint inversion profile appeared to find a balance between Rayleigh and Love wave profiles. The immediate near surface is very similar to Rayleigh waves, while the RMSE at depths of 4 m – 5 m matches that of Love wave results. From 4 m to 11 m, the joint inversion RMSE increases compared to Love waves, but offers an improvement over the Rayleigh wave profiles. At deeper strata, the joint inversion exhibits similar results to the Rayleigh and Love waves, except for the 45° impact which performed significantly better for Rayleigh waves. For joint inversion, the 15° impact had the lowest overall RMSE, while the 45° impact had the highest error.

Based on these observations related to the inverted V_S profiles, it appears that Love waves were less affected by changes in impact angle. The V_S profiles more closely matched the ground truth information and varied less with changes in impact angle compared to Rayleigh wave profiles. Uncertainty in the Love wave results was also significantly less. These results indicate that the optimal impact angle should be governed by Rayleigh waves, as the quality of the Rayleigh wave V_S results is more negatively impacted by changes in source angle. An impact angle that favors

vertical may produce the best results for $MAS_{RL}W$, although this conclusion could be site dependent.

4.6. Summary

Chapter 4 examined the effectiveness of an angled impact for simultaneous generation of Rayleigh and Love waves based on an analysis of *f*, power/energy levels, *SNR*, and V_S profiles. Frequency content present in a surface wave is an important parameter to ensure adequate coverage for development of a dispersion curve during MASW analysis. The frequency content of both Rayleigh and Love waves was examined based on peak power spectral density (PSD), f_{dom}, and bandwidth (using δ as a proxy). For Rayleigh waves, the 0° and 15° impacts generated the highest peak PSD when averaged across source offsets and receiver spacings. When using a 45° impact, the reduction in energy was more than 50%. However, the data still showed that Rayleigh wave energy was most affected by impact angle relative to Love waves. For Love waves, the peak PSD occurred for the 15° impact. The lower-than-expected PSD values for the 45° impact may have been due to source coupling issues. The 90° results could be explained by the smaller size of the sledgehammer used for this angle when compared to the AWD source for the other angles. Nevertheless, when comparing the 45° impact to the 0° impact, the difference in energy was usually less than 25%.

For both Rayleigh and Love waves, the f_{dom} shifted towards lower frequencies as the impact angle was moved away from their ideal orientation (i.e., 0° for Rayleigh, 90° for Love). For both Rayleigh and Love waves, larger bandwidths occurred as the impact was made more horizontal. The relative energy and *SNR* trends for Rayleigh and Love waves mirrored the observations made for PSD. The *SNR* did indeed seem less sensitive to impact angles though the average *SNR* across all channels did vary by more than 10% when comparing the different impact angles.

The effect of impact angle on dispersion image quality was also examined. The dispersion images of each impact angle were compared to the optimal dispersion image for that wave type. For Rayleigh waves, the best dispersion image was generated by a 0° impact. However, the dispersion curves from the 15° impact compared favorably to this optimal angle, particularly for *f* higher than 40 Hz. For Love waves, a 90° impact produced the best dispersion images. Overall, the dispersion images generated from Love wave data were much clearer than the dispersion images generated from Rayleigh waves. It was often difficult to identify an obvious fundamental mode in the Rayleigh wave overtones. Love wave dispersion curves were clear, and a fundamental mode could be identified even for the 0° dispersion images. These results indicate that the quality of Love wave overtones is less affected by changes in impact angle than Rayleigh wave overtones. Consequently, use of a purely vertical impact to generate usable Love wave data was possible at this site.

An inversion process was used to generate independently and jointly inverted V_S profiles for each impact angle of Rayleigh and Love wave testing. Each inverted V_S profile was compared to a V_S profile generated from ground truth information (i.e. seismic refraction and downhole testing).

Both Rayleigh and Love wave V_S profiles were substantially different from the ground truth information with a total minimum RMSE between the predicted and ground truth V_S of over 500 m/s. However, Rayleigh waves tended to perform better at shallow and larger depths, while Love waves performed better at intermediate depth strata. The 0° V_S profile matched the ground truth model most closely for Rayleigh waves when considering RMSE from ground truth as well as the amount of inversion uncertainty. For Love waves, both the 90° and 45° impacts performed similarly compared to the ground truth profile.

Overall, the Love wave profiles were closer to the ground truth model and suffered less uncertainty than the Rayleigh wave profiles. This applied to each impact angle of Love wave data. The joint inversion profile was an improvement over both Rayleigh and Love waves. The joint inversion procedure seemed to benefit from the quality of the predictions of Rayleigh waves at shallow strata and Love waves at deeper strata. Consequently, a 10% improvement in RMSE for jointly inverted V_S was realized. Uncertainty was also reduced, likely due to the additional constraints inherent in the joint inversion procedure. The 15° impact performed best at depth for the joint inversion profile and produced the lowest RMSE compared to ground truth information.

Based on these results, it appears that Love waves were generally less susceptible to changes in impact angle at the TAB site. For Love waves, each impact angle produced reasonable dispersion curves and V_S profiles. Therefore, an impact angle of 15°, which favors the generation of Rayleigh waves, may be ideal for the simultaneous generation of Rayleigh and Love waves. This angle produced reasonable dispersion curves and V_S profiles for both Rayleigh and Love waves. The 15° impact also generated peak power and SNR for Rayleigh waves and produced similar power and SNR when compared to the optimal strike for Love waves. After joint inversion of Rayleigh and Love waves, the 15° impact produced reasonably accurate V_S profiles and displayed the lowest RMSE compared to ground truth information.

With respect to MAS_LW using purely vertical impacts, the results of this study indicated that this approach was certainly feasible at this site. The relative energy information indicated that such a 0° strike generated 56.8% less energy than the most powerful strike (90° impact angle). Though a drastic difference, this was nevertheless a useable amount of Love wave energy by which to proceed with MAS_LW analysis. With respect to *SNR*, the 45° impact angle and 0° impact angle were often well within 25%. Finally, the RMSE between ground truth and the inverted V_S profile for the 0° impact angle was typically within 10% of the RMSE for the 45° impact angle. This was similar to the difference in RMSE exhibited between ground truth and the 90° and 45° impact models.

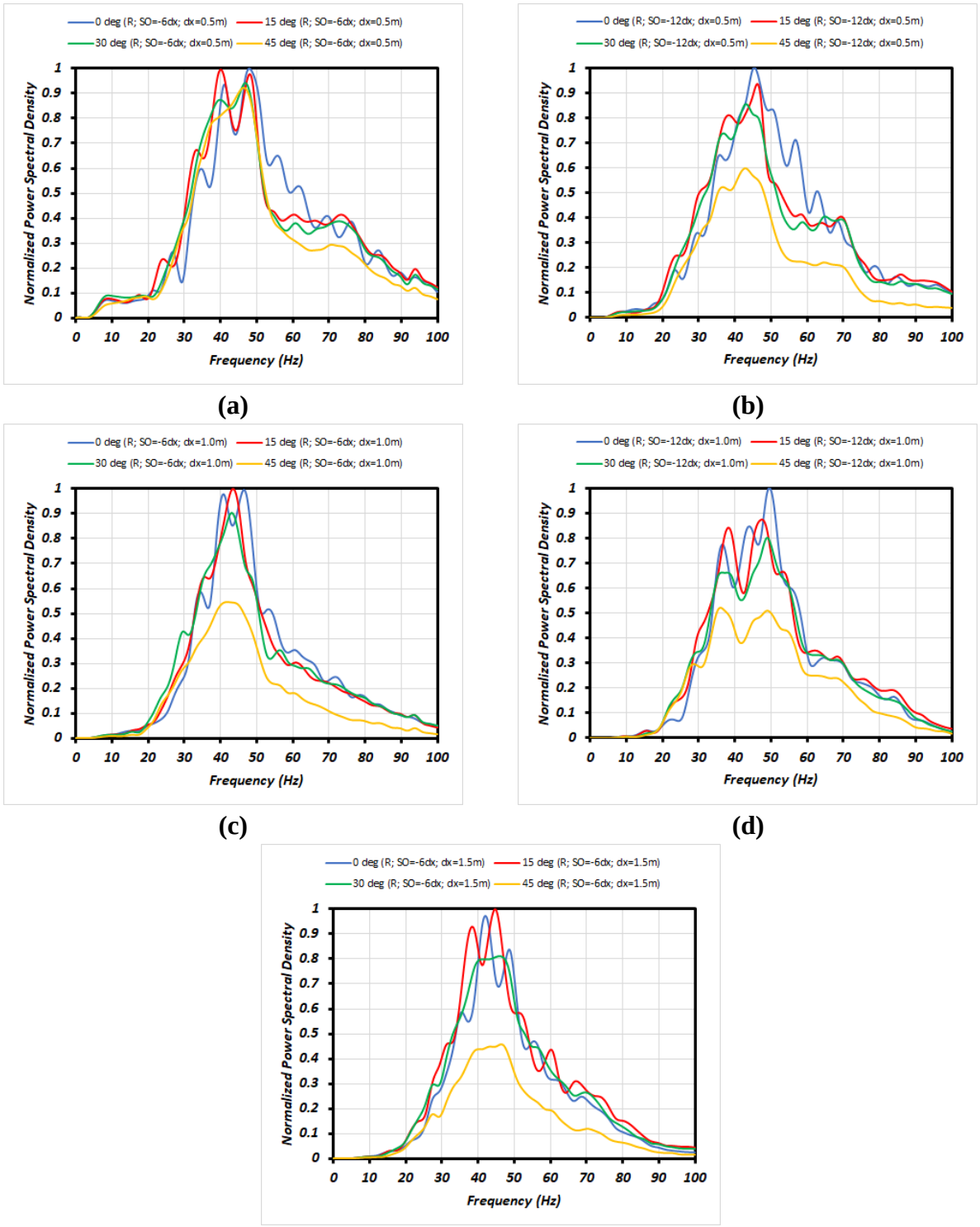

Figure 4.1. Normalized Rayleigh power spectral density plots: (a) SO = -6dx, dx = 0.5 m; (b) SO = -12dx, dx = 0.5 m; (c) SO = -6dx, dx = 1.0 m; (d) SO = -12dx, dx = 1.0 m; and (e) SO = -6dx, dx = 1.5 m.

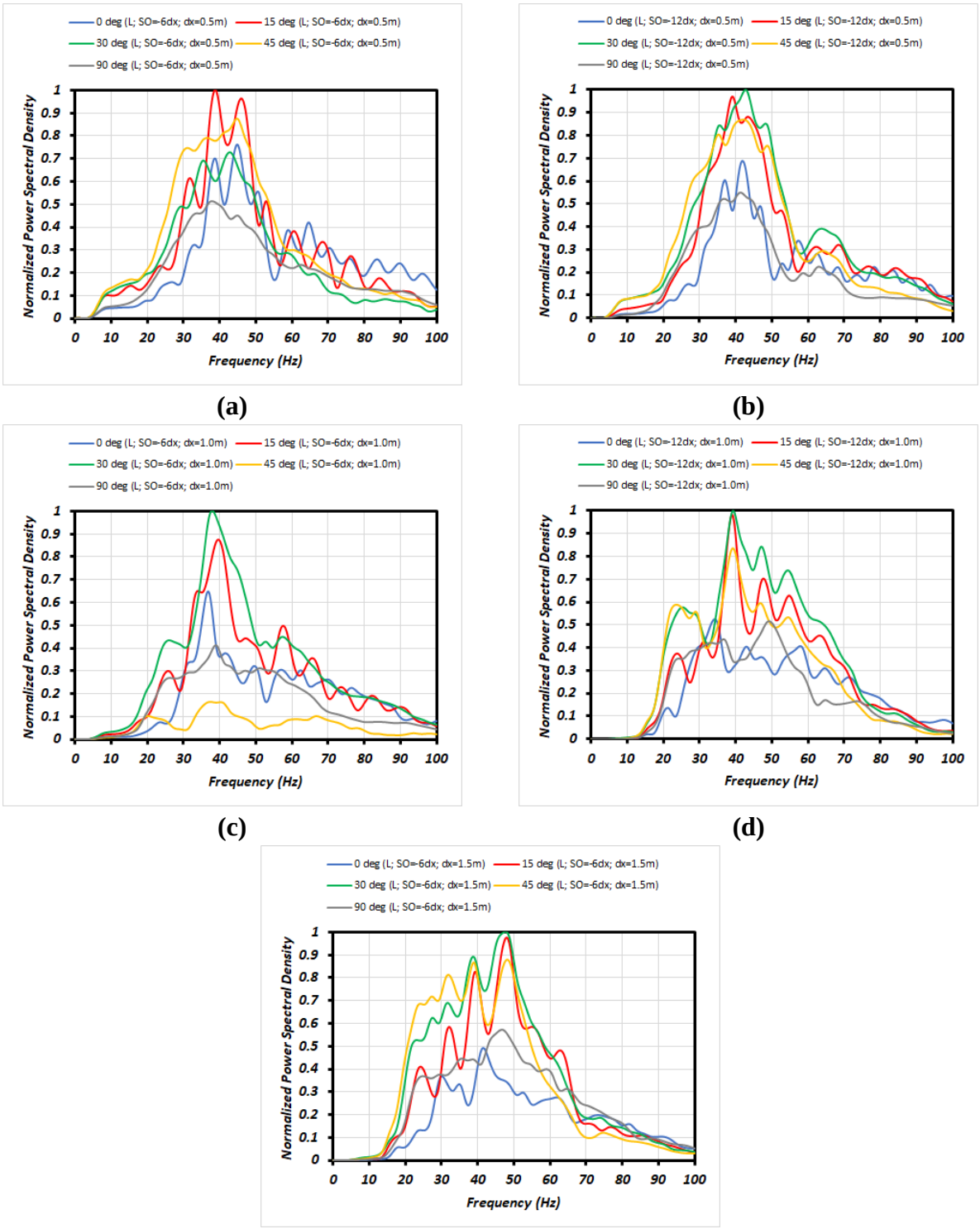

Figure 4.2. Normalized Love power spectral density plots: (a) SO = -6dx, dx = 0.5 m; (b) SO = -12dx, dx = 0.5 m; (c) SO = -6dx, dx = 1.0 m; (d) SO = -12dx, dx = 1.0 m; and (e) SO = -6dx, dx = 1.5 m.

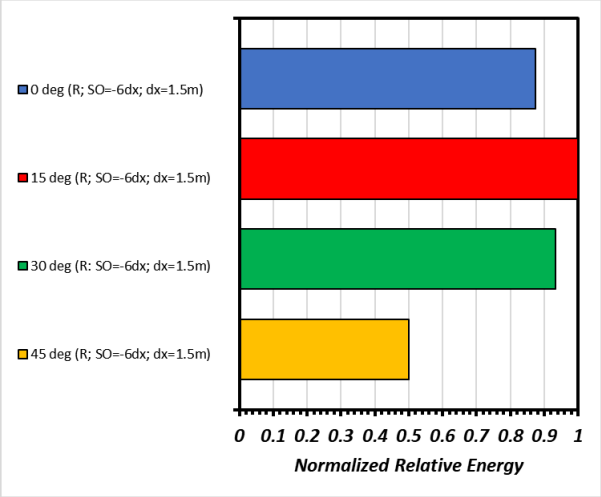

(a)

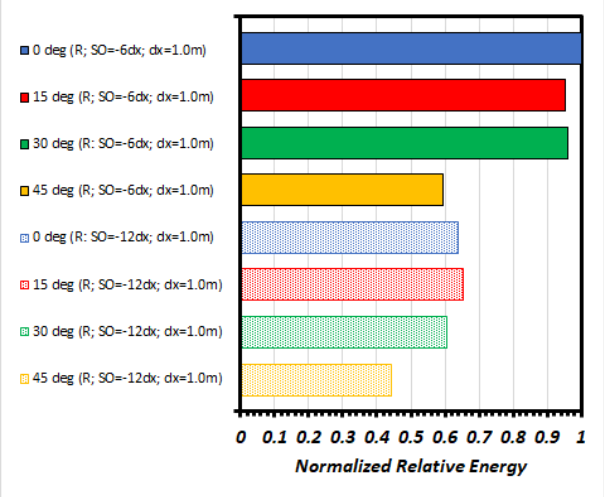

(b)

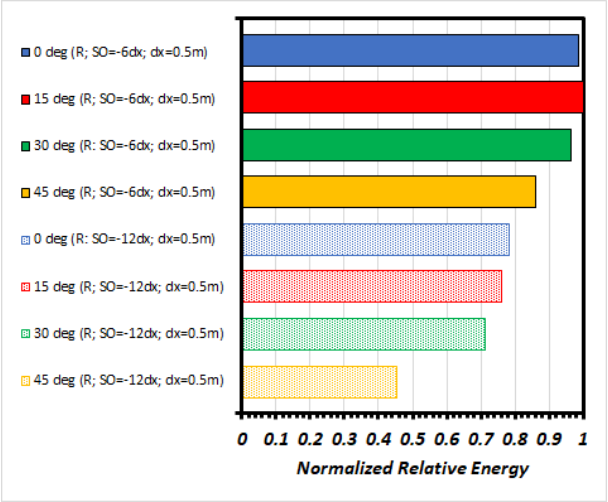

(c)

Figure 4.3. Normalized relative energy graphs of Rayleigh waves: (a) SO = -6dx, dx = 1.5 m; (b) SO = -6dx and -12dx, dx = 1.0 m; (c) SO = -6dx and -12dx, dx = 0.5 m.

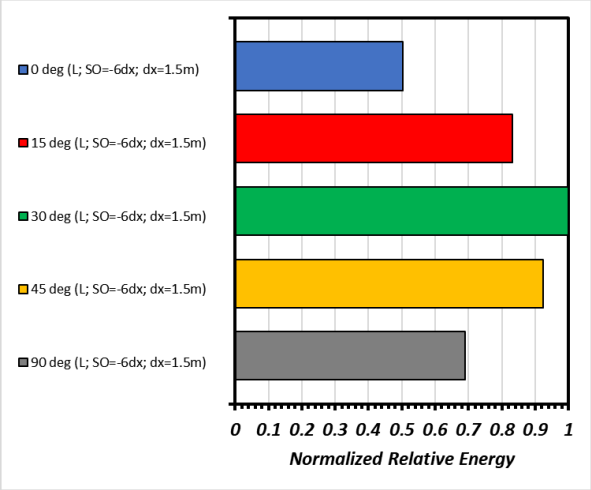

(a)

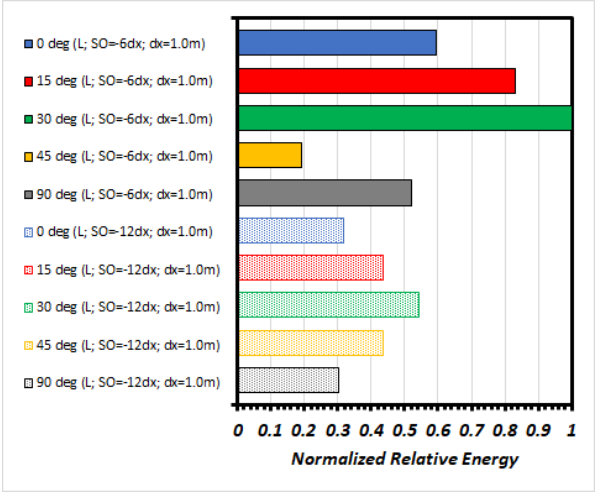

(b)

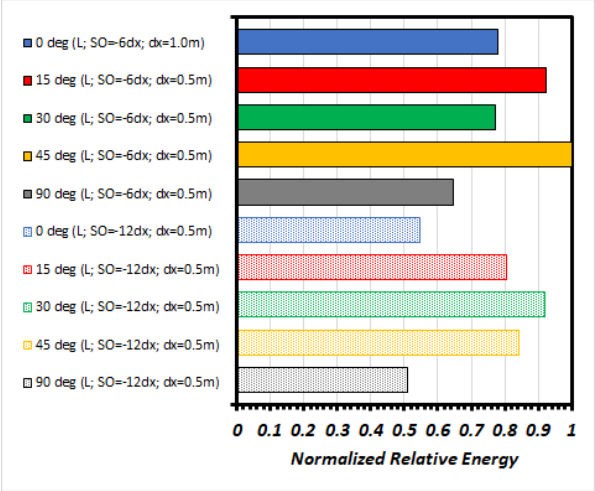

(c)

Figure 4.4. Normalized relative energy graphs of Love waves: (a) SO = -6dx, dx = 1.5 m; (b) SO = -6dx and -12dx, dx = 1.0 m; (c) SO = -6dx and -12dx, dx = 0.5 m.

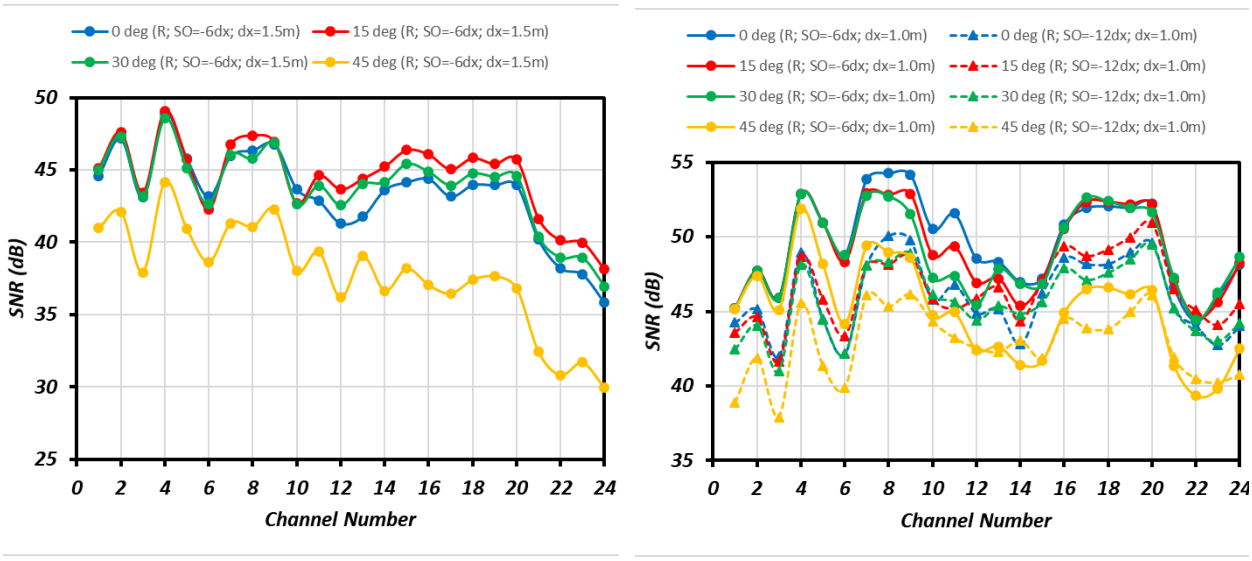

(a) **(b)**

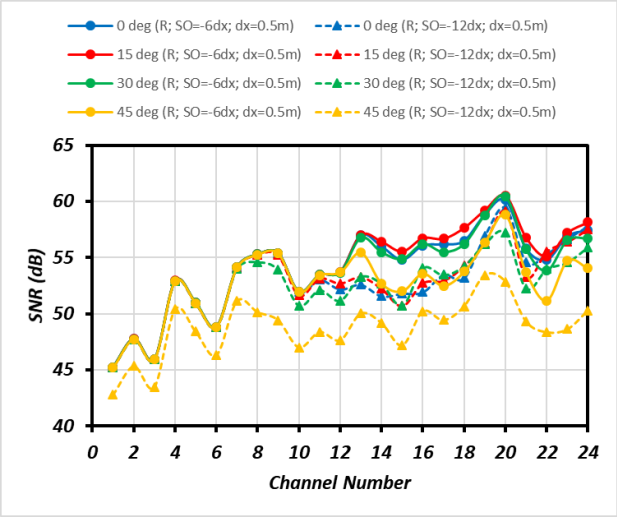

(c)

Figure 4.5. SNR plots of Rayleigh waves: (a) SO = -6dx, dx = 15 m; (b) SO = -6dx and -12dx, dx = 1.0 m; (c) SO = -6dx and -12dx, dx = 0.5 m.

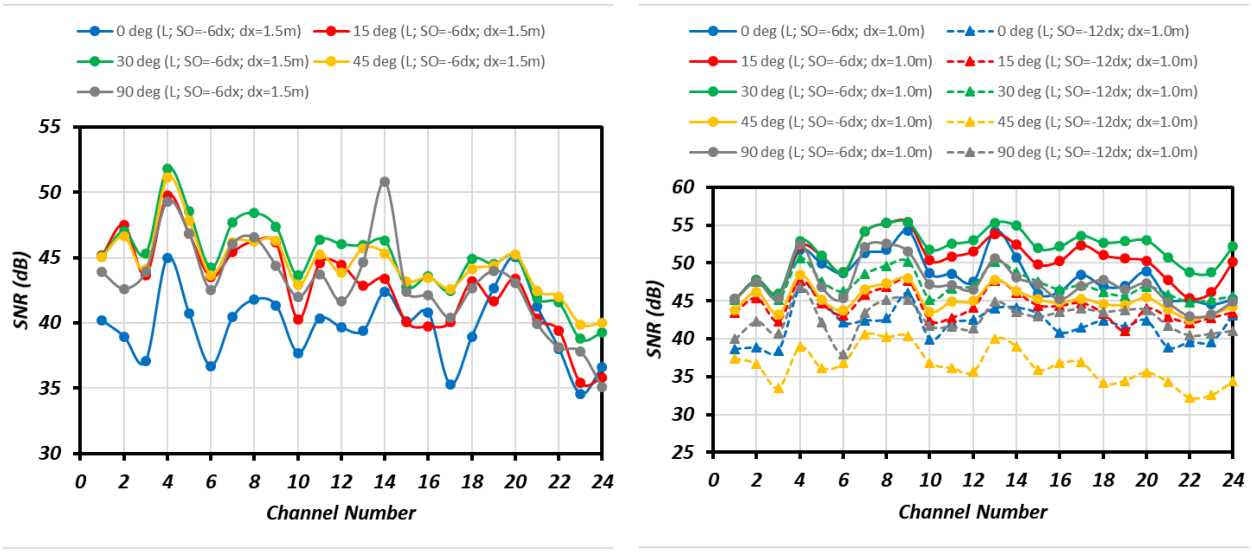

(a) **(b)**

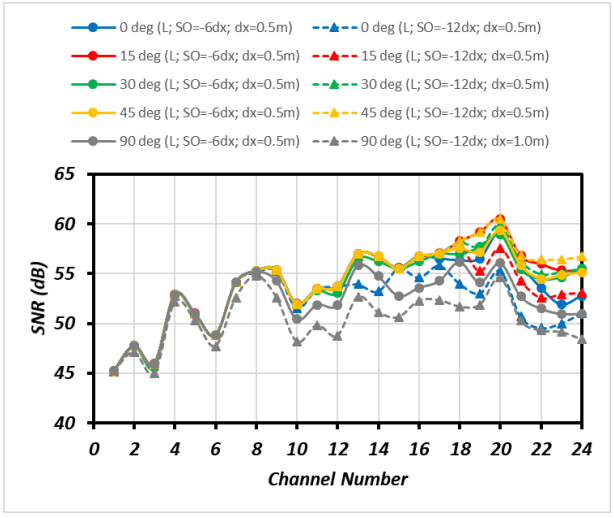

(c)

Figure 4.6. SNR plots of Love waves: (a) SO = -6dx, dx = 1.5 m; (b) SO = -6dx and -12dx, dx = 1.0 m; (c) SO = -6dx and -12dx, dx = 0.5 m.

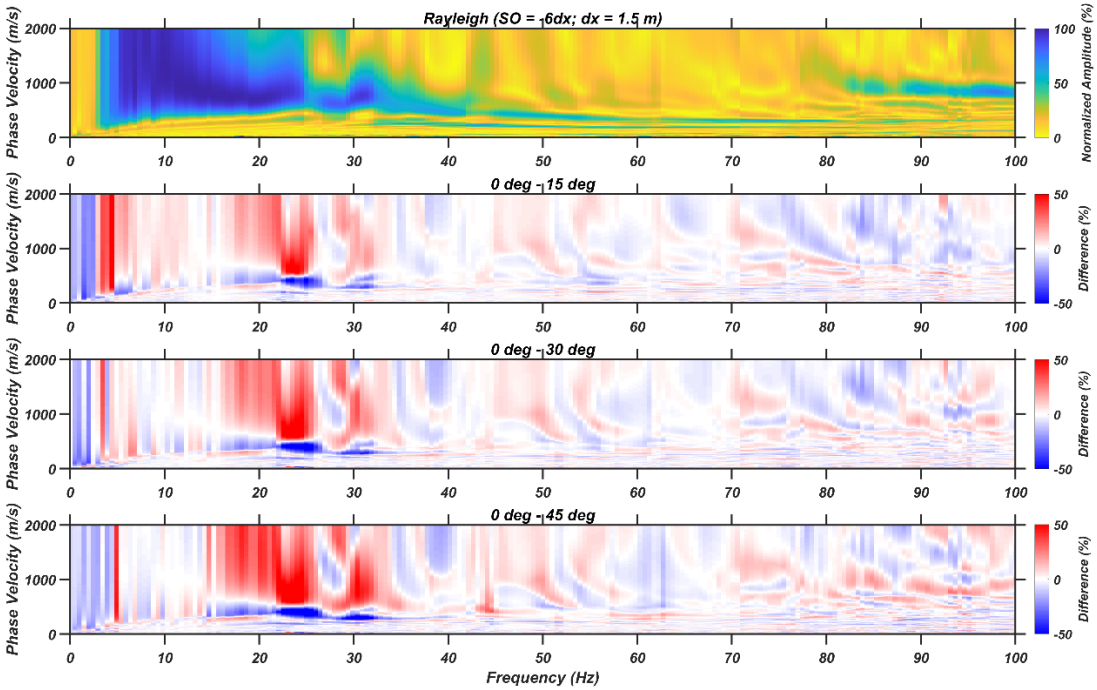

(a)

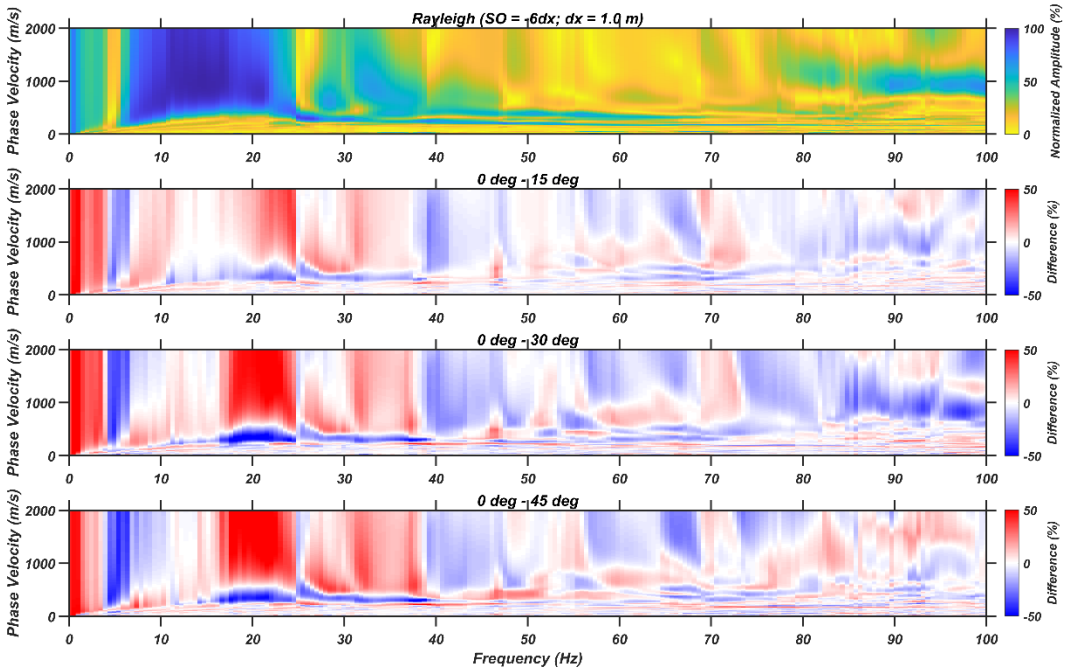

(b)

Figure 4.7. Rayleigh wave dispersion curves compared to the 0° dispersion image: (a) SO = -6dx, dx = 1.5 m; (b) SO = -6dx, dx = 1.0 m.

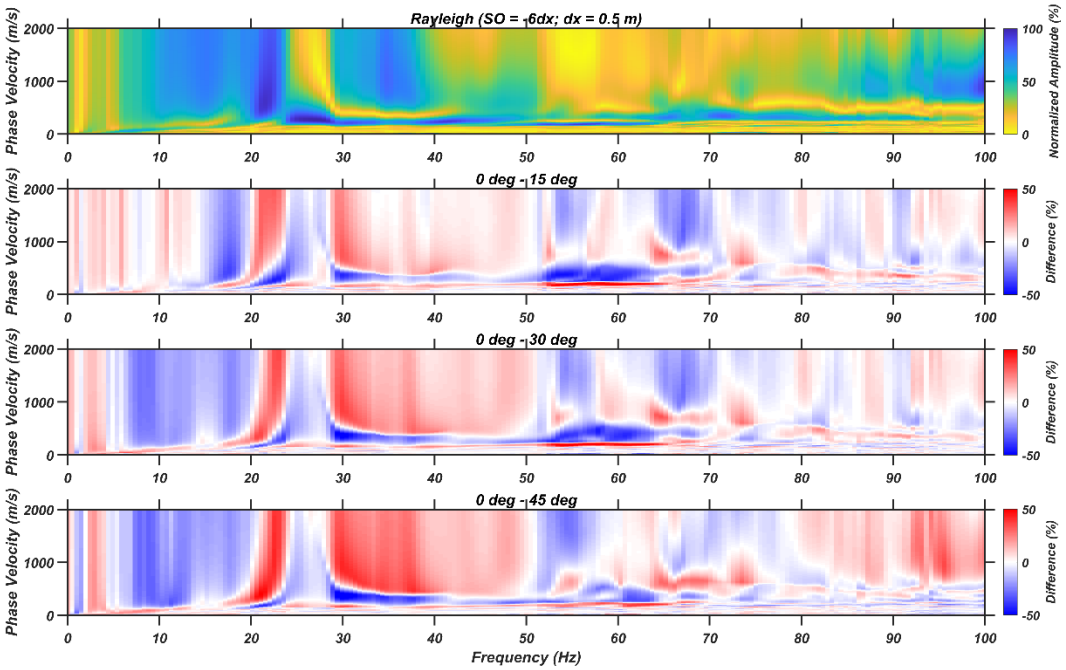

(c)

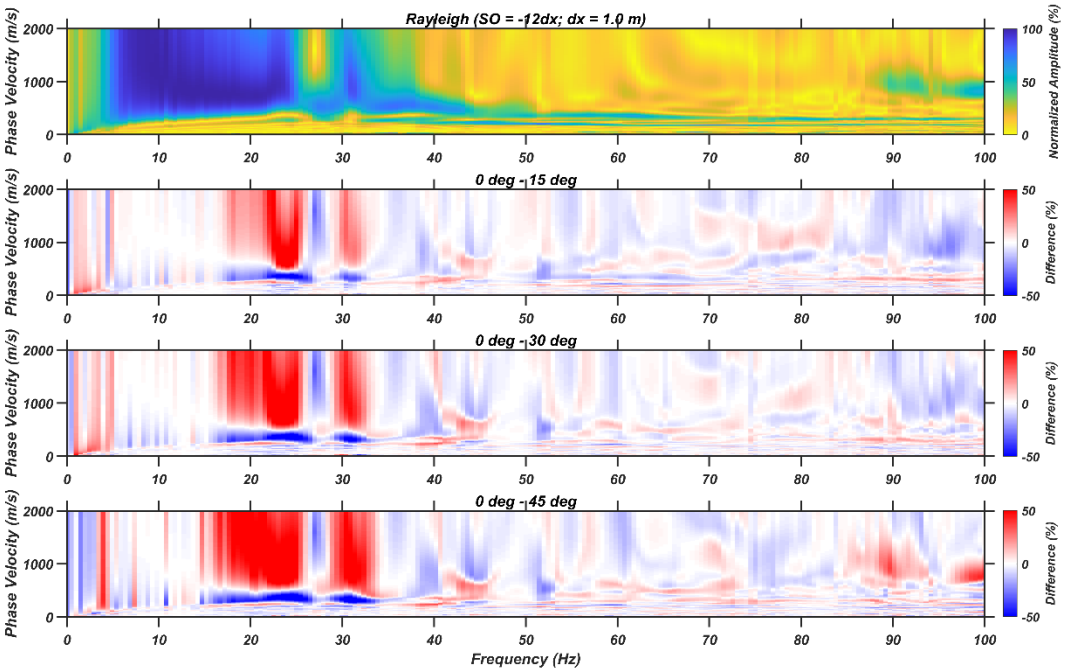

(d)

Figure 4.7 (cont.). Rayleigh wave dispersion curves compared to the 0° dispersion image: (a) SO = -6dx, dx = 0.5 m; (b) SO = -12dx, dx = 1.0 m.

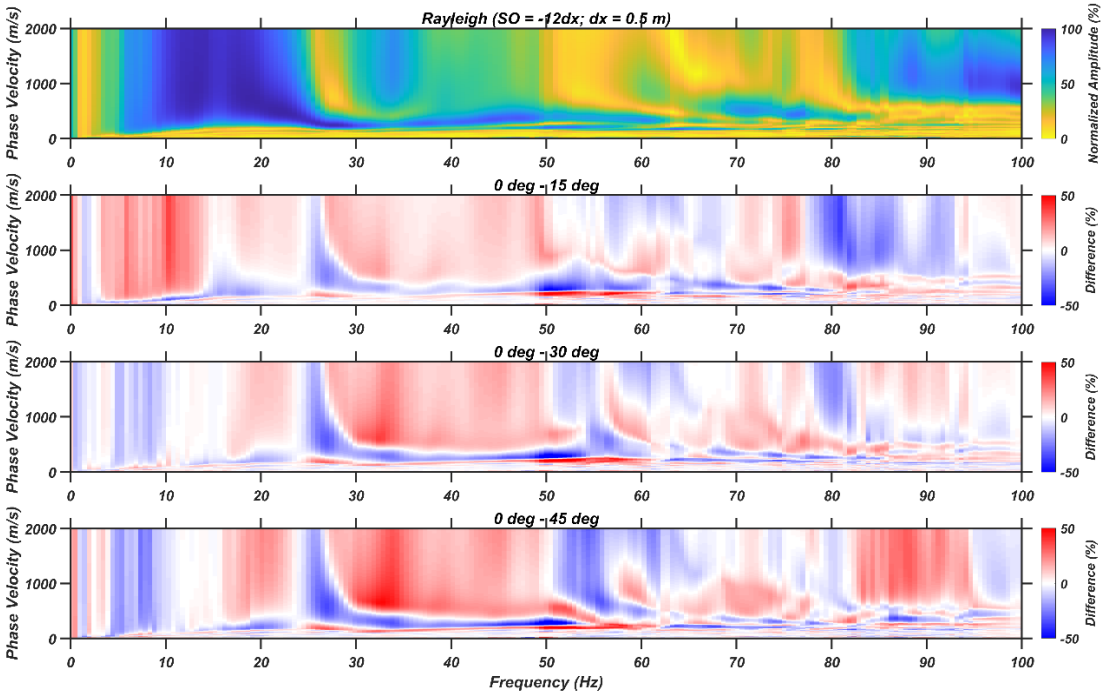

(e)

Figure 4.7 (cont.). Rayleigh wave dispersion images compared to the 0° dispersion image: (e) SO = -12dx, dx = 0.5 m.

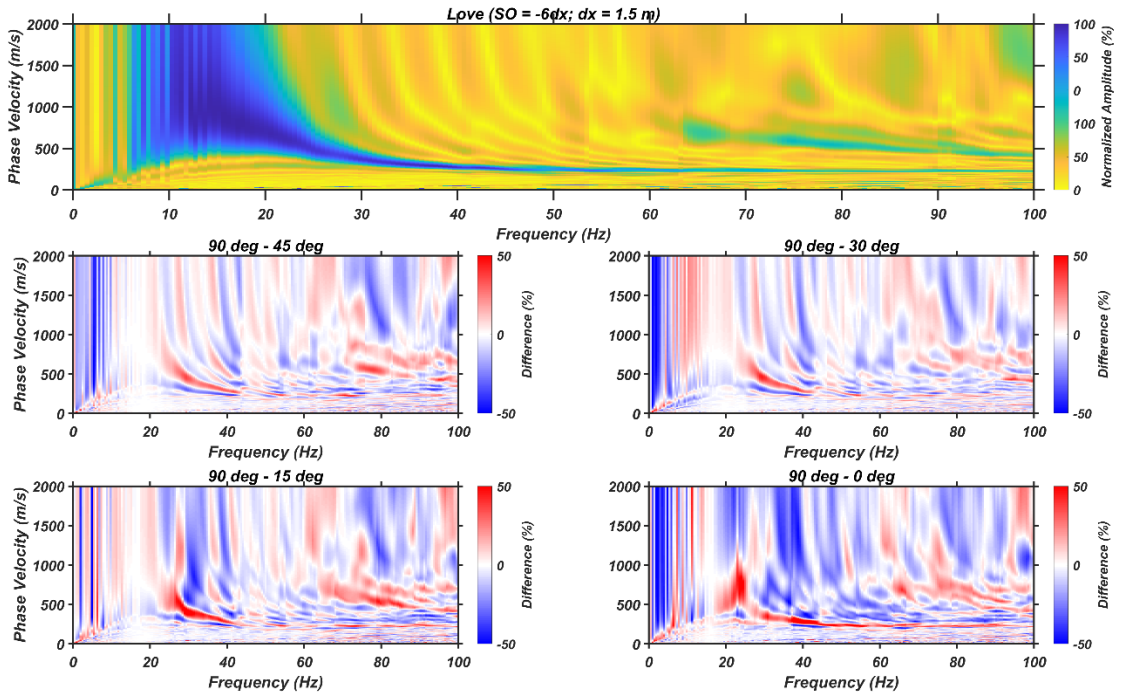

(a)

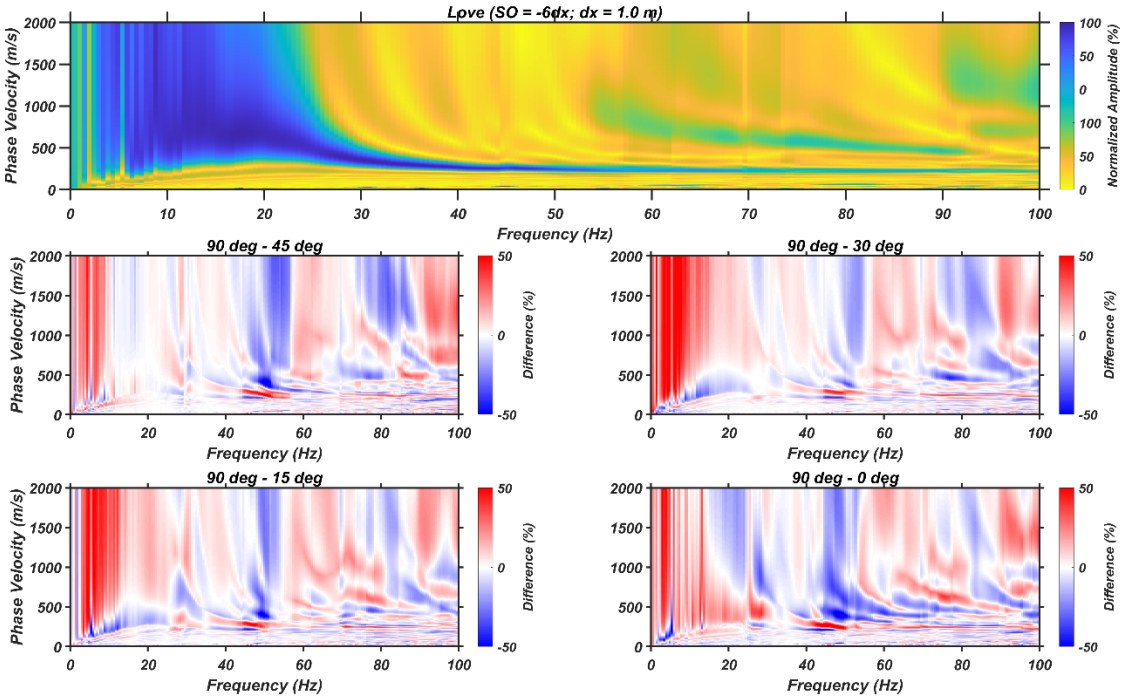

(b)

Figure 4.8. Love wave dispersion images compared to the 0° dispersion image: (a) SO = -6dx, dx = 1.5 m; (b) SO = -6dx, dx = 1.0 m.

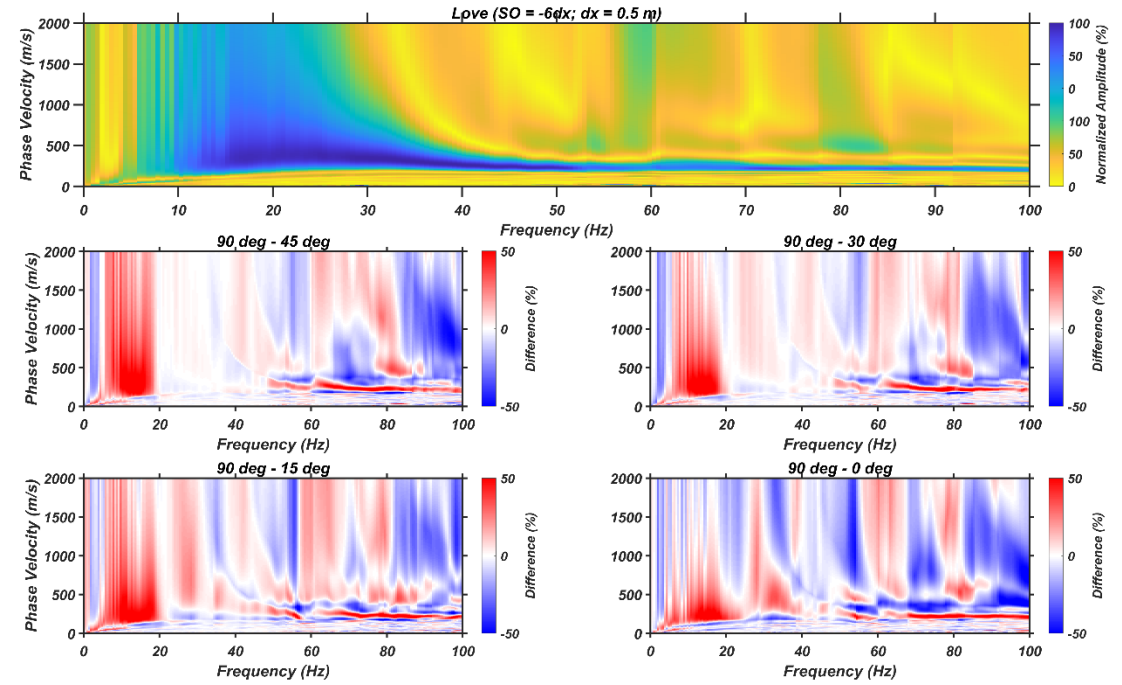

(c)

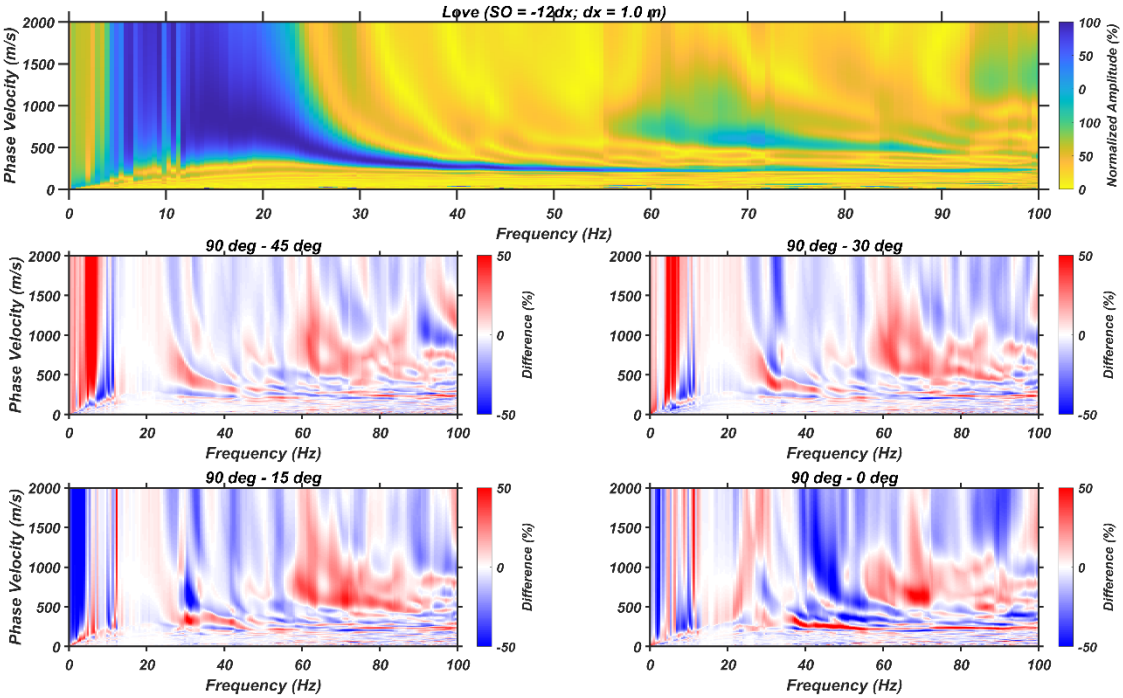

(d)

Figure 4.8 (cont.). Love wave dispersion images compared to the 0° dispersion image: (c) SO = -6dx, dx = 0.5 m; (d) SO = -12dx, dx = 1.0 m.

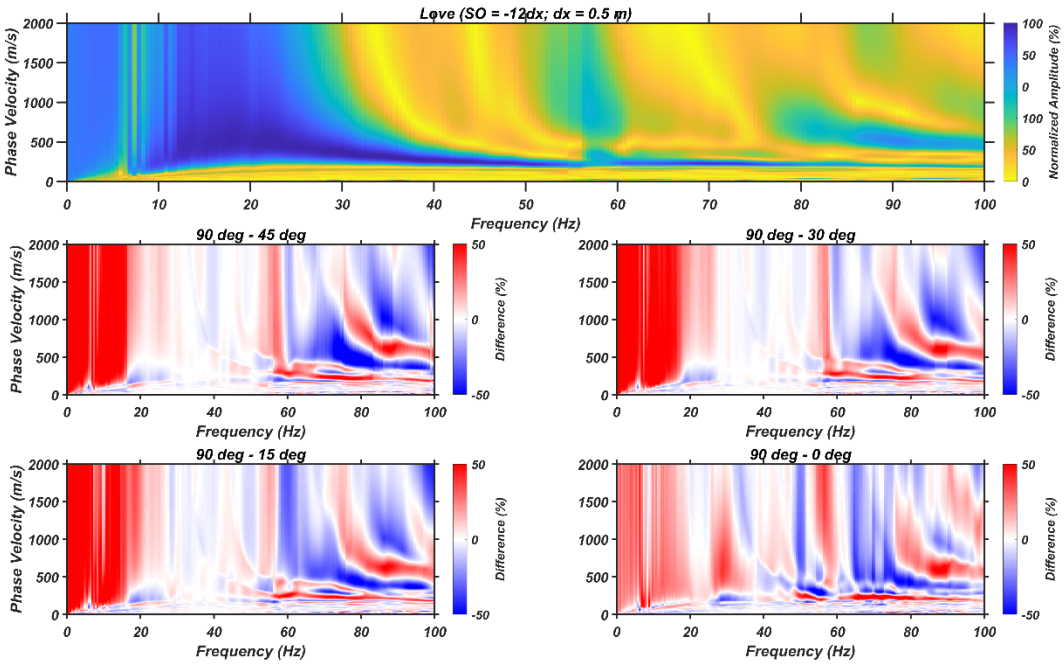

(e)

Figure 4.8 (cont.). Love wave dispersion images compared to the 90° dispersion image: (e) SO = -12dx, dx = 0.5.

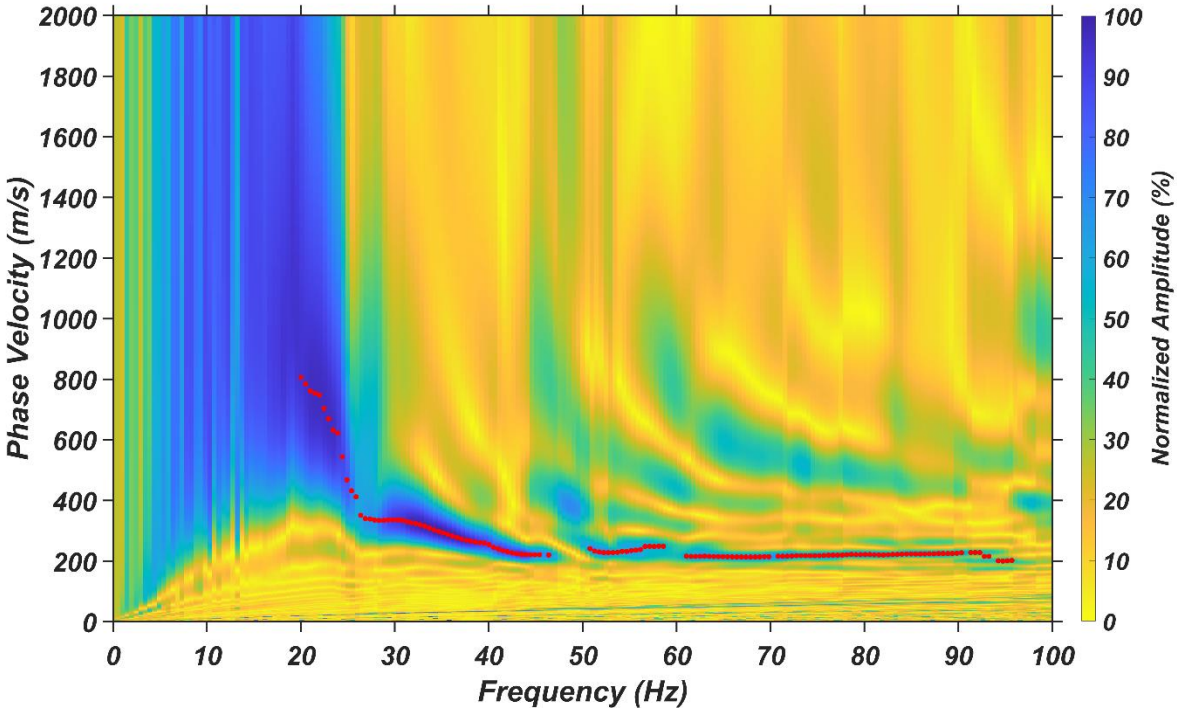

Figure 4.9. Love wave dispersion curve generated by a 0° impact.

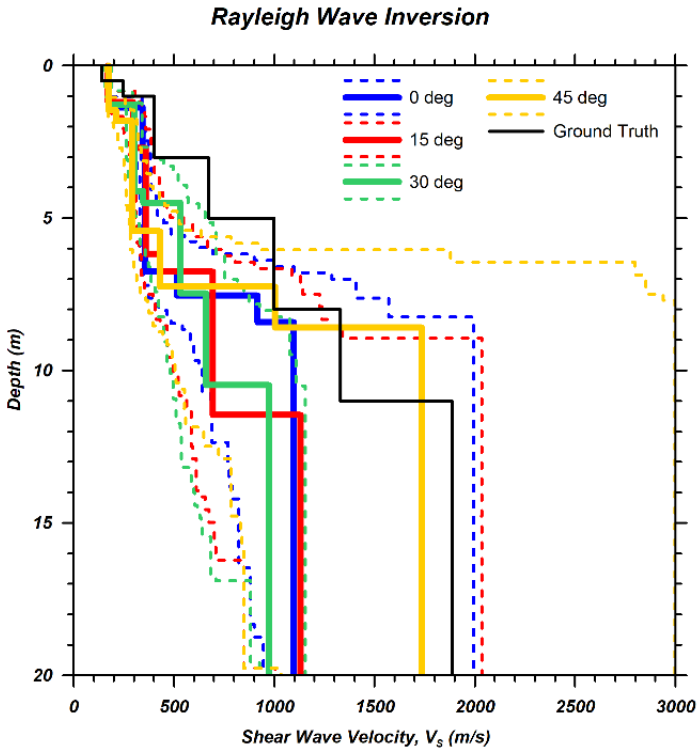

(a)

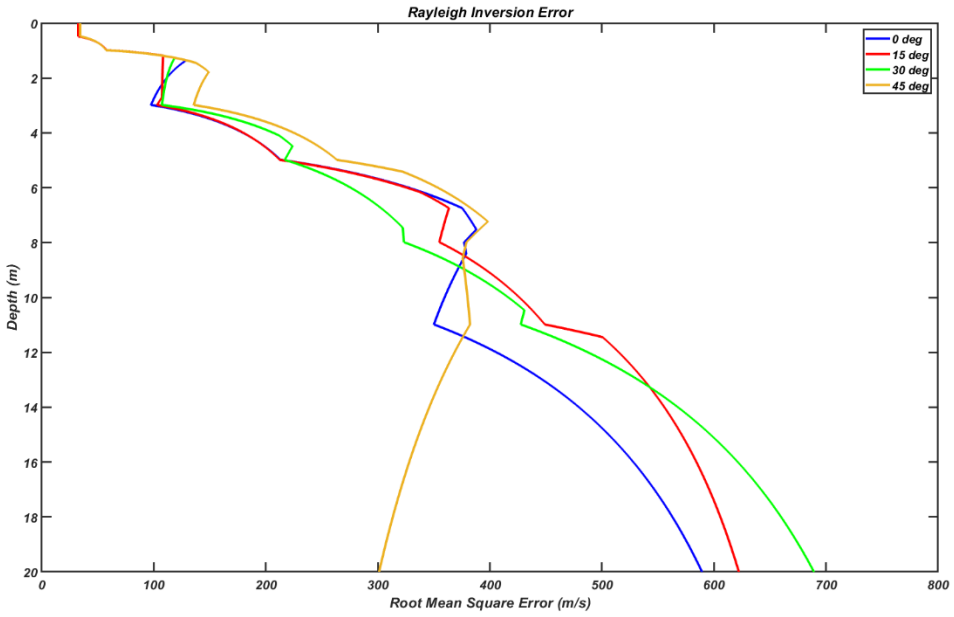

(b)

Figure 4.10. Rayleigh inversion: (a) V_S profiles; and (b) difference between inverted V_S and ground truth model V_S.

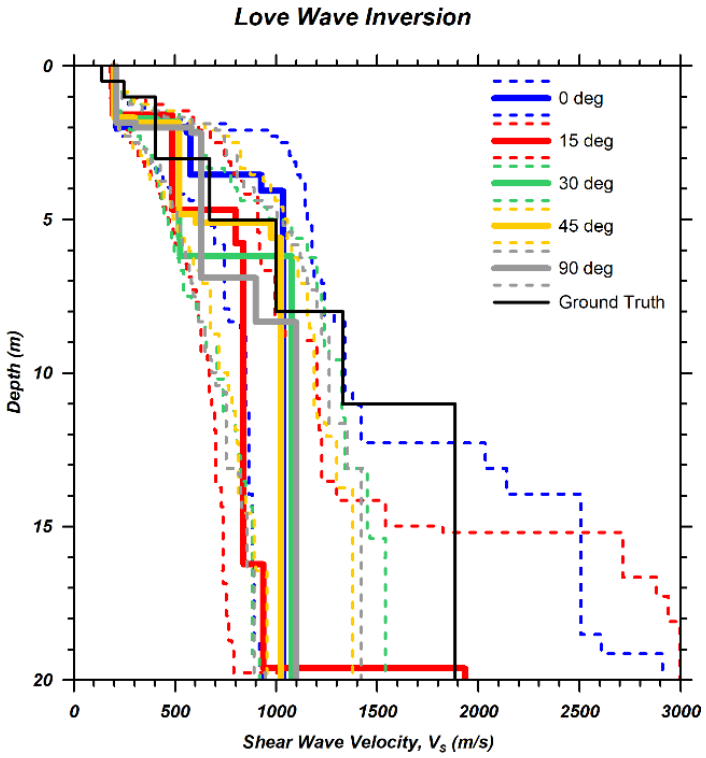

(a)

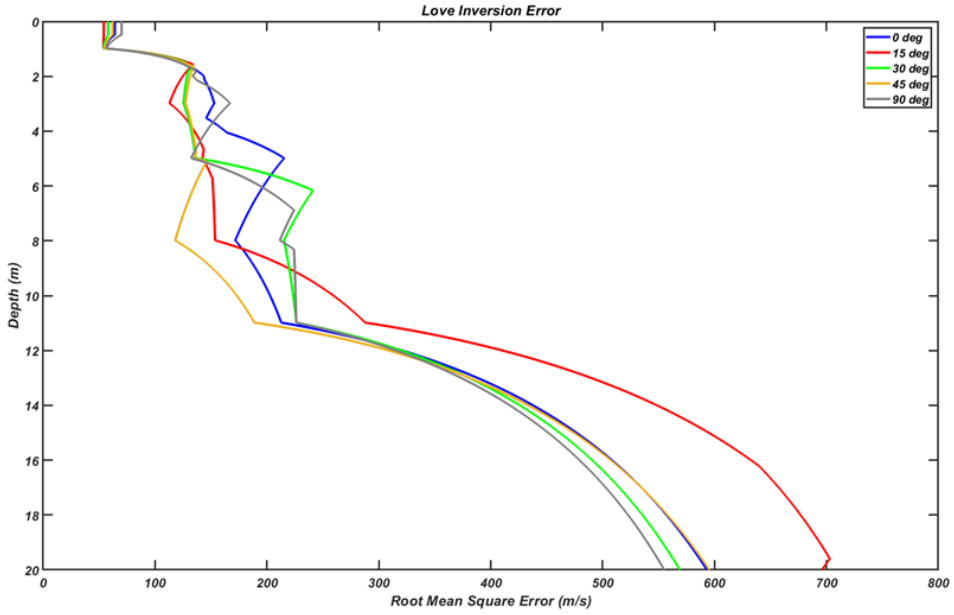

(b)

Figure 4.11. Love wave inversion: (a) V_S profiles; and (b) difference between inverted V_S and ground truth model V_S.

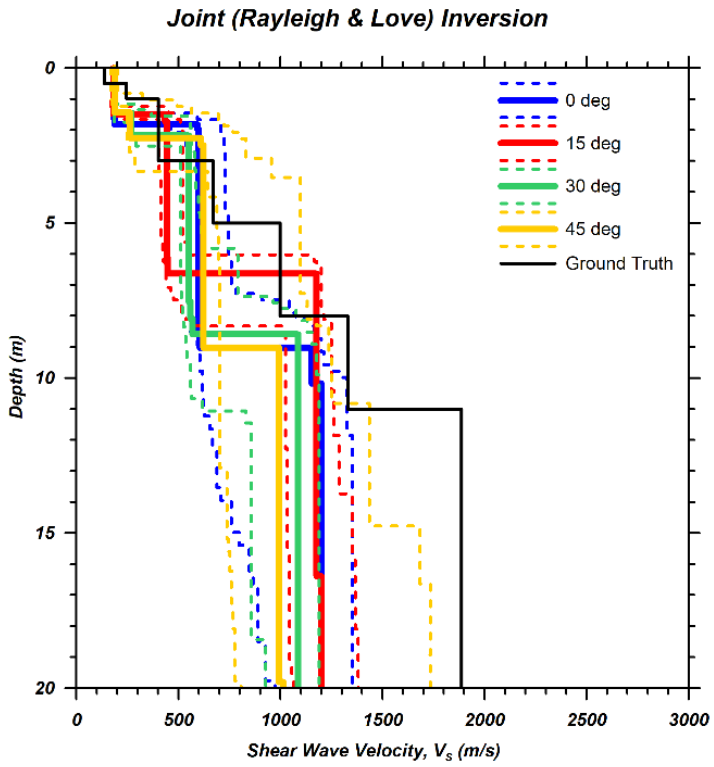

(a)

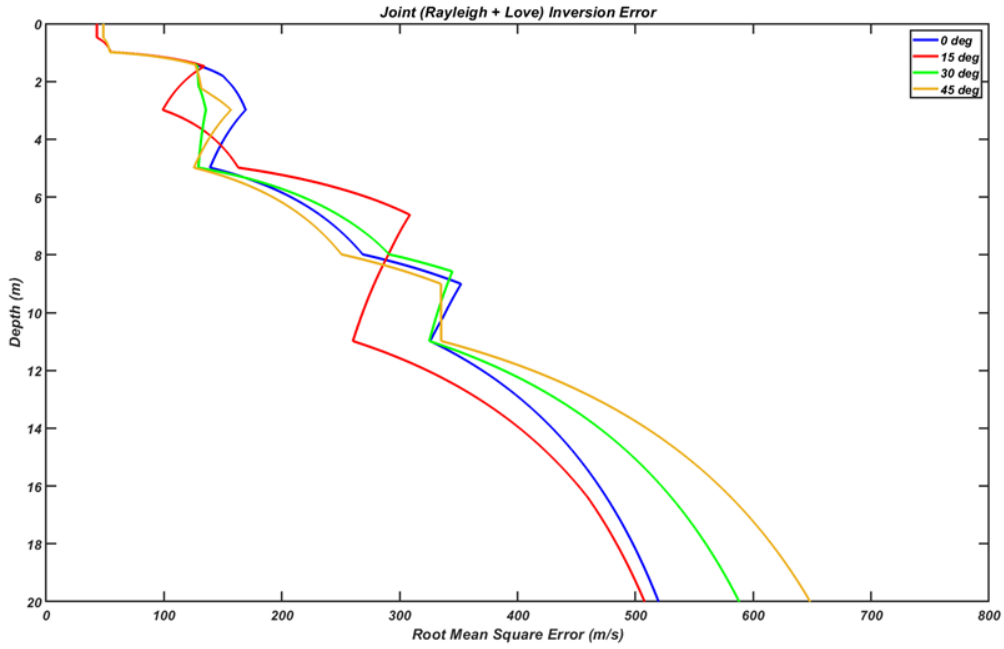

(b)

Figure 4.12. Joint (Rayleigh and Love) inversion: (a) V_S profiles; and (b) difference between inverted V_S and ground truth model V_S.

Table 4.1. Dominant frequencies in PSD plots for Rayleigh waves.

SO	dx	0°	15°	30°	45°
- 6*dx*	0.5 m	48.0	40.0	46.8	46.4
-12*dx*		45.4	46.1	43.1	42.9
- 6*dx*	1.0 m	46.4	43.4	43.1	41.9
-12*dx*		49.5	47.4	48.9	36.0
- 6*dx*	1.5 m	42.0	44.6	45.9	46.3
Average		46.26	44.3	45.56	42.7
Difference (%)			-4.2%	-1.5%	-7.7%

Table 4.2. Shape factors (δ) from PSD plots for Rayleigh waves.

SO	dx	0°	15°	30°	45°
- 6*dx*	0.5 m	0.330	0.353	0.355	0.343
-12*dx*		0.318	0.345	0.340	0.328
- 6*dx*	1.0 m	0.308	0.322	0.333	0.321
-12*dx*		0.295	0.316	0.311	0.317
- 6*dx*	1.5 m	0.294	0.312	0.309	0.308
Average		0.309	0.330	0.329	0.323
Difference (%)			6.5%	6.5%	4.5%

Table 4.3. Dominant frequencies in PSD plots for Love waves.

SO	dx	90°	45°	30°	15°	0°
- 6*dx*	0.5 m	37.9	44.7	42.7	38.7	44.8
-12*dx*		41.3	42	42.7	39	41.8
- 6*dx*	1.0 m	38.9	37.4	37.9	39.6	36.7
-12*dx*		49.2	39.2	39.3	38.9	34.1
- 6*dx*	1.5 m	46.7	48.1	47.6	47.9	41.5
Average		42.8	42.28	42.04	40.82	39.78
Difference (%)			-1.2%	-1.8%	-4.6%	-7.1%

Table 4.4. Shape factors (δ) from PSD plots for Love waves.

SO	dx	0°	15°	30°	45°	
- 6*dx*	0.5 m	0.385	0.381	0.381	0.368	0.350
-12*dx*		0.371	0.365	0.362	0.358	0.351
- 6*dx*	1.0 m	0.365	0.392	0.363	0.354	0.338
-12*dx*		0.357	0.354	0.337	0.329	0.347
- 6*dx*	1.5 m	0.352	0.360	0.345	0.327	0.345
Average		0.366	0.370	0.358	0.347	0.346
Difference (%)			1.1%	-2.3%	-5.2%	-5.4%

5. CONCLUSIONS

The MASW method is becoming an increasingly popular method of surface wave testing due to its non-destructive nature and potential to create accurate V_S profiles. Studies continue to advance the methodology but have typically focused on utilizing Rayleigh waves. Several studies have shown that Love waves can offer distinct advantages over Rayleigh waves. To obtain the best MASW results, data from both Rayleigh and Love waves should be collected. V_S profiles may then be created by independent and joint inversion, which reduces the uncertainty inherent in the inversion process. However, the process of collecting Rayleigh and Love wave data separately significantly increase data acquisition time when using standard MASW procedures because they are polarized in different directions and require different input sources. Therefore, this study examined the effectiveness of simultaneous inversion of Rayleigh and Love waves using angled impacts. Impact angles have been analyzed based on *f*, *SNR*, dispersion information, and V_S profiles. This research also examined the effectiveness of vertical impacts for Love wave generation.

MASW field testing was performed to examine the effectiveness of an angled impact for the simultaneous generation of Rayleigh and Love waves. Testing was performed at a baseball field at the Temple Ambler campus site (TAB) approximately 24 km north of Center City Philadelphia. A set of 24 geophone receivers was used to collect surface wave data from impacts were performed at angles of 0°, 15°, 30°, 45°, and 90°. The 90° impact was not used to generate Rayleigh waves due to logistical issues. An AWD was used to produce impacts on all sources but the 90° source, where a 20 lb sledgehammer was utilized.

Following data collection, data was processed using a combination of custom MATLAB scripts, the Geometrics SeisImager/SW® commercial software package, and the open-source Geopsy software package. The phase-shift method (Park et al., 1998) was used to generate dispersion images and both independent and joint inversions were performed to produce V_S profiles. These V_S profiles were subsequently compared to ground truth information obtained from previous seismic refraction and downhole testing.

5.1. Goals of Project

The goals of this research effort were to provide recommendations regarding the optimal impact angle for the simultaneous generation of Rayleigh and Love wave and to examine the effectiveness of a vertical strike for Love wave generation. The following conclusions can be drawn after an analysis of *f*, power, *SNR*, dispersion curves, and V_S profiles:

- A 15° impact produced the highest normalized relative energy for Rayleigh waves. A 30° impact produced the highest normalized relative energy for Love waves. However, a 15° impact generated just 11.8% less energy for Love waves. A 15° impact also produced the highest *SNR* and f_{dom} for Rayleigh waves. The 15° impact performed within 5% of the optimal angle (i.e. 30°) for Love wave generation. Therefore, at the TAB site, a 15° impact

is recommended for maximum energy during simultaneous generation of Rayleigh and Love waves.

- A vertical strike (i.e., 0°) generated 56.8% less Love wave energy than the most powerful strike at 30 degrees.
- Dominant frequencies and *SNR* were only moderately affected by changes in impact angle for both Rayleigh and Love waves. Average f_{dom} and average *SNR* changed by no more than 10% between different impact angles.
- The Love wave dispersion curve generated by vertical strikes matched reasonably well with the dispersion curve generated by an ideal impact angle (i.e., 90°). This result indicates that vertical strikes may be effective for Love wave generation.
- The Love wave overtone images were significantly clearer than the Rayleigh wave images, especially in terms of fundamental-mode identification. Love wave dispersion curves also matched reasonably well between different data sets, even as the impact angle approached vertical.
- Neither Rayleigh nor Love waves provided V_S profiles that matched well with the ground truth model. Rayleigh waves performed well at the near surface, however, uncertainty and misfit increased with depth. Love waves performed better overall, particularly in the intermediate range of depths. Love wave V_S profiles were also significantly less impacted by changes in impact angle.
- Overall, Love waves were less affected by changes in impact angle. Because Rayleigh waves are more affected by source angle at the TAB site, the optimal impact angle should be governed by Rayleigh waves.

This research effort showed that, at the TAB site examined in this study, Love waves were significantly less affected by changes in impact angle than were Rayleigh waves. Even as the impact angle moved towards vertical, Love wave generation still occurred and reasonable dispersion images were obtained. This conclusion may prove valid across a wide range of site conditions due to the inherent properties of Love wave generation. Near-vertical impacts seem to produce sizable horizontal wave components, especially as the wave propagates farther from the impact source. This effect may be caused by the restorative force of gravity that pulls near-vertical waves towards horizontal. Love wave generation could benefit significantly from this effect and, as a result, the optimal angle for simultaneous generation may be inclined more towards vertical.

6. REFERENCES

Abbiss, C.P. (1981). "Shear wave measurements of the elasticity of the ground." *Geotechnique*, 31(1), 91-109.

Cox, B. R., and Teague, D. P. (2016). "Layering ratios: a systematic approach to the inversion of surface wave data in the absence of a priori information." *Geophysical Journal International*, 207(1), 422-438.

Dal Moro, G., and Ferigo, F. (2011). "Joint analysis of Rayleigh-and Love-wave dispersion: Issues, criteria and improvements." *Journal of Applied Geophysics*, 75(3), 573-589.

Eslick, R., Tsoflias, G., and Steeples, D. (2007). "Field investigations of Love waves in near-surface seismology." *Geophysics*, 73(3), G1–G6.

Foti, S., Hollender, F., Garofalo, F. et al. (2018). "Guidelines for the good practice of surface wave analysis: a product of the InterPACIFIC project." *Bull. Earthquake Eng*., 16, 2367–2420.

Gaiser, J. (2016). *3C Seismic and V_SP: Converted waves and vector wavefield applications.* Society of Exploration Geophysicists, Tulsa, OK, 636 pp.

Haines, S. S. (2007). *A hammer-impact, aluminum, shear-wave seismic source*. Open-File Report 2007–1406, U.S. Department of Interior, U.S. Geological Survey, Reston, VA.

Hardage, B. A., DeAngelo, M. V., Murray, P. E., and Sava, D. (2011). *Multicomponent seismic technology.* Society of Exploration Geophysicists, Tulsa, OK, 335 pp.

Häusler, M., Schmelzbach, C., and Sollberger, D. (2018). "The Galperin source: A novel efficient multicomponent seismic source." Geophysics, 83(6), P19-P27.

Heisey, J.S., Stokoe II, K.H., and Meyer, A.H. (1982). "Moduli of pavement systems from Spectral Analysis of Surface Waves." *Transp. Res. Rec.*, 852, 22-31.

Jones, R. (1955). "A Vibration Method for Measuring the Thickness of Concrete Road Slabs In Situ." *Magazine of Concrete Research*, 7(20), 97-102.

Jones, R. (1958). "In situ measurement of the dynamic properties of soil by vibration methods." *Geotechnique*, 8(1), 1-21.

Julia, J., Ammon, C.J., Herrman, R.B., and Correig, A.M. (2000). "Joint inversion of receiver function and surface wave dispersion observations." *Geophysical Journal International*, 143, 99–112.

Lay, T., and Wallace. T. C. (1995). *Model Global Seismology*. Oxford, United Kingdom, Academic Press.

J.L. Mari. (1984). "Estimation of static corrections for shear-wave profiling using the dispersion properties of Love waves." *Geophysics*, 49(8), 1169-1179.

Kramer, S.L. (1996). *Geotechnical Earthquake Engineering*. Pearson, New Jersey, 653 pp.

Love, A.E. (1911). *Some problems of geodynamics*. Cambridge University Press.

Mahvelati, S., (2019). *Advancements in Surface Wave Testing: Numerical, Laboratory, and Field Investigations Regarding the Effects of Input Source and Survey Parameters on Rayleigh and Love Waves.* Ph.D. Dissertation, Temple University.

Mahvelati, S. and Coe., J. T. (2017). "Multichannel Analysis of Surface Waves (MASW) Using Both Rayleigh and Love Waves to Characterize Site Conditions." *Proceedings Geotechnical Frontiers*, 647-656.

Matthews, M.C., Hope, V.S. and Clayton, C.R.I. (1996). "The use of surface waves in the determination of ground stiffness profiles." *Proc. Institution of Civil Engineers Geotech. Engineering*., 119, 84-95.

Miller, R.D., Pullan, S.E., Waldner, J.S., and Haeni, F.P. (1986). "Field comparison of shallow seismic sources." *Geophysics*, 51(11), 2067-2092.

McMechan, G. A., and Yedlin, M. J. (1981). "Analysis of dispersive waves by wave field transformation." *Geophysics*, 46(6), 869-874.

Ólafsdóttir, Á. E. (2014). *Multichannel Analysis of Surface Waves: Methods for dispersion analysis of surface wave data.* University of Iceland: School of Engineering and Natural Sciences, 76 pp.

Olafsdottir, E. A., Bessason, B., and Erlingsson, S. (2018). "Combination of dispersion curves from MASW measurements." *Soil Dynamics and Earthquake Engineering*, 113, 473-487.

Park, C.B., Miller, R.D., and Xia, J. (1998). "Imaging dispersion curves of surface waves on multi-channel record." *68th Ann. Internat. Mtg. Soc. Expl. Geophys*., 1377-1380.

Park, C.B., Miller, R.D., and Miura H. (2002). "Optimum field parameters of an MASW survey." *Japanese Society of Exploration Geophysics Extended Abstracts*, 1-6.

Park, C.B., Miller, R.D., Xia, J., and Ivanov., J. (2007). "Multichannel analysis of surface waves (MASW) – active and passive methods." *The Leading Edge*, 26(1), 60-64.

Pei, D. (2007). *Modeling and inversion of dispersion curves of surface waves in shallow site investigations*. Ph.D Dissertation, University of Nevada, Reno.

Rossi, G., and Vesnaver, A. (1997). "3-D imaging by adaptive joint inversion of reflected and refracted arrivals." *SEG Technical Program Expanded Abstracts*, 1873-1876.

Safani, J., O'Neill, A., Matsuoka, T., and Sanada, Y. (2005). "Applications of Love wave dispersion for improved shear-wave velocity imaging." *Journal of Environmental Engineering Geophysics*, 10(2), 135–150.

Schmelzbach, C., Sollberger, D., Greenhalgh, S. A., Horstmeyer, H., Maurer, H., and Robertsson, J. O. (2016). "9C seismic data acquisition for near-surface applications: Recording, waveform reciprocity and 4C rotation." *78th EAGE Conference and Exhibition*, 1-5.

Socco, L.V., Foti, S., and Boiero, D. (2010). "Surface-wave analysis for building near-surface velocity models – Established approaches and new perspectives." *Geophysics*, 75(5), 75A83-75A102.

Song, Y. Y., Castagna, J. P., Black, R. A., and Knapp, R. W. (1989). "Sensitivity of Near-Surface Shear-Wave Velocity Determination from Rayleigh and Love Waves." *Proc. SEG 59th Ann. Mtg.*, Dallas, TX, 509-512.

Tokimatsu, K., Kuwayama, S., Tamura, S. and Miyadera, Y. (1991). "V_S determination from steady state Rayleigh wave method." *Soils and Foundations*, 31(2), 153-163.

Van der Pol, C. (1951). "Dynamic Testing of Road Constructions." *Journal of Applied Chemistry*, 1, 281-290.

Vanmarcke, E.H. (1976). "Structural response to earthquakes." *Seismic Risk and Engineering Decisions*, C. Lomnitz and E. Rosenblueth (Eds.), 287-338.

Vozoff, K., and Jupp, D.L.B. (1975). "Joint Inversion of Geophysical Data." *Geophys. J. Int.*, 42, 977–991.

Wathelet, M. (2005). *Array Recordings of Ambient Vibrations: Surface-wave Inversion*. PhD Dissertation, Liège University, 177 pp.

Wathelet, M. (2008). "An improved neighborhood algorithm: parameter conditions and dynamic scaling." *Geophysical Research Letters*, 35, L09301, doi: 10.1029/2008GL033256.

Wathelet, M., Chatelain, J.-L., Cornou, C., Di Giulio, G., Guillier, B., Ohrnberger, M. and Savvaidis, A. (2020). "Geopsy: A User-Friendly Open-Source Tool Set for Ambient Vibration Processing." *Seismological Research Letters*, 91(3), 1878–1889.

Xia, J., Miller, R. D., and Park, C. B. (2000). "Advantages of calculating shear-wave velocity from surface waves with higher modes." *SEG Technical Program Expanded Abstracts*, 1295-1298.

Xia, J., Xu, Y., Luo, Y., Miller, R. D., Cakir, R., and Zeng, C. (2012). "Advantages of using multichannel analysis of Love waves (MALW) to estimate near-surface shear-wave velocity." *Surveys in Geophysics*, 33(5), 841-860.

Xia, J., Miller, R. D., and Park, C. B. (1999). "Estimation of near-surface shear-wave velocity by inversion of Rayleigh waves." *Geophysics*, 64(3), 691–700.

Yin, X., Xia, J., Shen, C., and Xu, H. (2014). "Comparative analysis on penetrating depth of high-frequency Rayleigh and Love waves." *J. Appl. Geophys*., 111, 86-94.

Yong, A., Martin, A., Stokoe, K., and Diehl, J. (2013). *ARRA-Funded V_{S30} Measurements Using Multi-Technique Approach at Strong-Motion Stations in California and Central-Eastern United States.* U.S. Geological Survey Open-File Report 2013–1102, 60 p. and data files, http://pubs.usgs.gov/of/2013/1102/.

Yoon, S., and Rix, G. J. (2009). “Near-field effects on array-based surface wave methods with active sources.” *Journal of Geotechnical and Geoenvironmental Engineering*, 135(3), 399-406.